Energy Conversion and Management 249 (2021) 114832

Contents lists available at ScienceDirect

Energy Conversion and Management

journal homepage: www.elsevier.com/locate/enconman

# Integration assessment of the hybrid sulphur cycle with a copper production plant

Ahmad Seyfaee [a,*], Mehdi Jafarian [a,*], Gkiokchan Moumin [b], Dennis Thomey [b], Claudio Corgnale [c], Christian Sattler [b], Graham J. Nathan [a]

[a] Centre for Energy Technology, School of Mechanical Engineering, University of Adelaide, Australia
[b] Institute of Future Fuels, German Aerospace Center (DLR), Germany
[c] Greenway Energy, USA

ARTICLE INFO

*Keywords:*
Hydrogen production
Sulphur cycle
Copper
Solar energy
Carbon dioxide emissions

ABSTRACT

Copper is the third-most widely-used metal worldwide. However, copper processing is an energy-intensive process consuming large quantities of fossil fuels, both as the reducing agent and for energy which contributes significantly to anthropogenic carbon dioxide emissions. The hybrid sulphur cycle combines concentrating solar thermal energy with electrolysis to offer strong potential for low-cost green hydrogen production. A preliminary evaluation is reported of the techno-economic potential of this cycle to displace current fossil-based energy sources in an integrated copper mine and refinery (cradle-to-gate approach) at a remote location in Australia with an excellent solar resource. The effect of ore composition on the integration of the hybrid sulphur cycle and copper processing plant is evaluated using models developed in Aspen Plus. The evaluations show that sizing the hybrid sulphur cycle cycle to meet the oxygen demand of the copper refining process is more techno-economically viable than sizing the hybrid sulphur cycle to meet the hydrogen required to replace the fossil fuel demand of the copper processing process. Moreover, it has been found that the integration of the hybrid sulphur cycle with the copper process plant has the potential to decrease both the carbon dioxide emissions and the operational expenditure of copper refineries for ores with a sufficiently high sulphide content (~50% mass fraction).

## 1. Introduction

There is growing interest in possible pathways to cost-effectively decarbonise the production of copper, which is the third-most widely-used metal with a current global demand of 18 million metric tonnes per year [1]. Currently, most of the energy required for copper processing is supplied from fossil fuels. Typically, 3.5–8 tonnes of carbon dioxide ($CO_2$) are produced per tonne of copper product, depending on the composition of the initial raw materials and its refinery process [2]. In particular the $CO_2$ emissions through the copper refining increase as the copper content of the ore decreases [3]. Hence, as the grade of the copper resources continues to fall, it is estimated that the specific $CO_2$ emission will rise to more than 10 tonnes of $CO_2$ per tonne of copper (Cu) product by 2033 [1,4]. For this reason, there is a strong need to identify cost-effective pathways with strong potential to mitigate the life-cycle $CO_2$ emissions associated with copper refining.

In the copper refining process (Fig. 1 (a)), the mined rock is first ground in a crushing unit [5] and then separated, typically via a flotation unit, into sulphide-containing (chalcocite ($Cu_2S$), covellite (CuS) and chalcopyrite ($CuFeS_2$)), and oxide-containing (tenorite (CuO) and cuprite ($Cu_2O$)) products. The sulphide ore is processed via a pyrometallurgical pathway, in which the heat of combustion of a hydrocarbon fuel (e.g. liquefied petroleum gas or LPG) in an oxygen-enriched environment is employed to produce industrially pure copper and sulphur dioxide ($SO_2$) in smelters and fire refiners (the direct to blister method). Hence, the pyrometallurgical pathway requires, in addition to the fossil fuel, oxygen enriched air, which is typically produced via an air separation unit (ASU), e.g. by cryogenic air separation or pressure swing adsorption (PSA). The copper-containing oxide ore stream ($Cu_2O$ and CuO) is treated via the hydrometallurgical pathway, in which sulphuric acid is employed to dissolve copper oxides and other traces of low content metals, e.g. uranium oxides. The dissolved copper ions are extracted via a solvent extraction process (SE) and deposited using the electrowinning process [6–8]. Typically part or all of the required

* Corresponding authors.
*E-mail addresses:* Ahmad.Seyfaee@Adelaide.edu.au (A. Seyfaee), Mehdi.Jafarian@Adelaide.edu.au (M. Jafarian).

https://doi.org/10.1016/j.enconman.2021.114832
Received 15 June 2021; Accepted 28 September 2021
Available online 23 October 2021

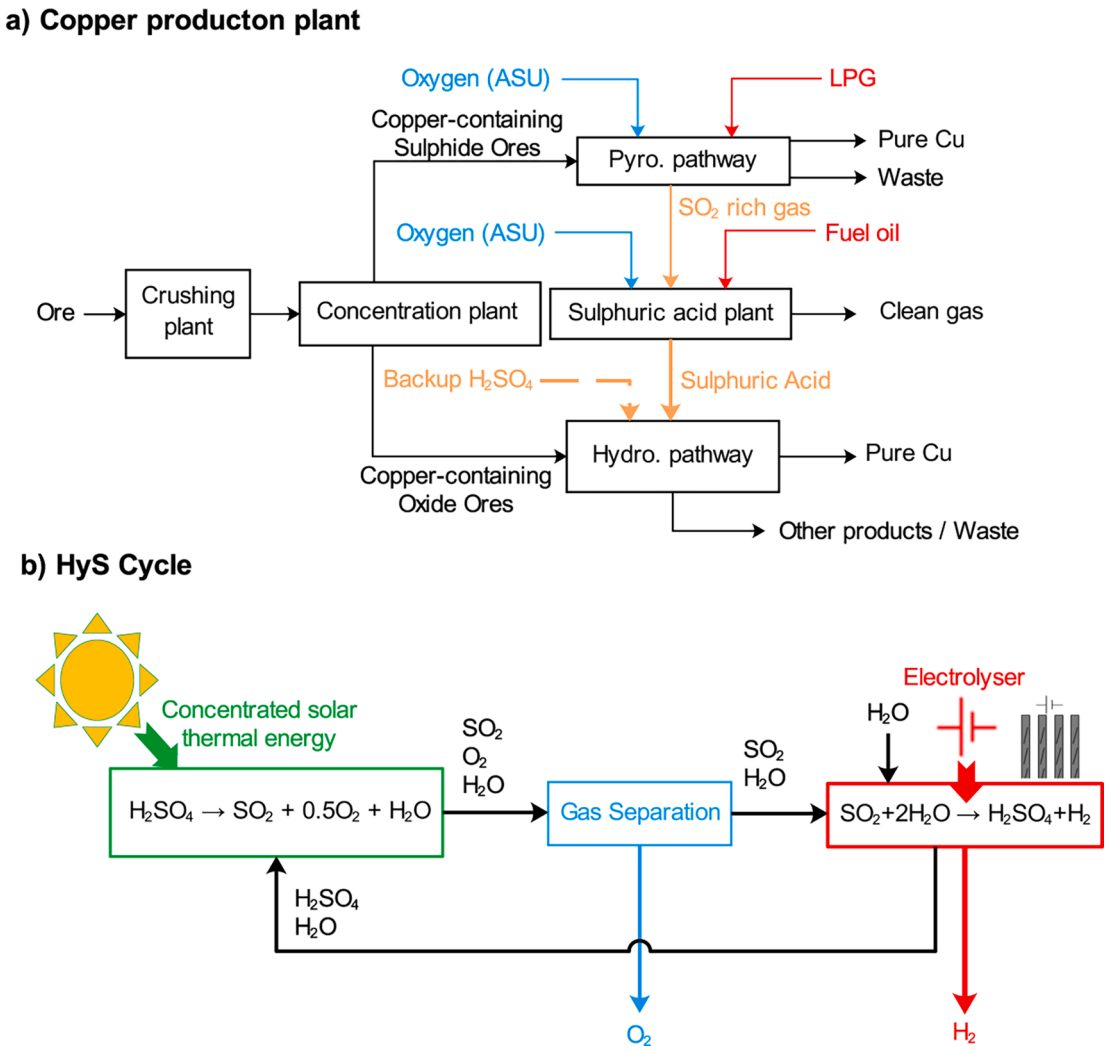


**Fig. 1.** Schematic diagrams of (a) copper refining process including pyrometallurgy and hydrometallurgy pathways [5,21,22] (b) HyS cycle for $H_2$ and $O_2$ production [23].

sulphuric acid in the hydrometallurgical pathway is produced in the acid plant, where the $SO_2$ off-gas from the furnaces in the pyrometallurgy pathway (e.g. smelters) is converted into sulphuric acid with the aid of a fuel (e.g. fuel oil) and oxygen from ASU unit.

One potential approach to mitigate the $CO_2$ emissions from the copper processing plants is to replace both the hydrocarbon fuel and oxygen (which is usually supplied by either air separation units (ASU) or pressure swing adsorption (PSA) technology) demand with high-grade hydrogen ($H_2$) and oxygen ($O_2$) supplied by water electrolysers, provided that their energy requirement is supplied from renewable resources. This has recently been ivestigated at the Atacama Desert in Chile by Gallardo et al. [9] for alkaline or polymer electrolyte membrane electrolysers with photovoltaic (PV) cells and concentrated solar thermal plants (CSP) with thermal energy storage (TES). They studied the potential for the export of produced $H_2$ in remote areas and showed that the combination of PV and electrolyser could be economically viable if a buffer such as hydrogen storage is available. Even more recently the techno-economic potential of decarbonising the copper production with $H_2$ supplied through retrofitting of water electrolyses to copper processing has been explored [10] and it was found that under the current techno-economic parameters for Germany, the cost of $CO_2$ abatement is approximately 326 AuD/t $CO_2$-eq. An alternative method to co-produce hydrogen and oxygen with renewable energy from water is the Hybrid Sulphur (HyS) cycle, which is a hybrid between a high-temperature heat source, e.g. concentrated solar thermal energy, and electricity. The HyS cycle has already been demonstrated at technology readiness level (TRL) 5 by the German Aerospace Center, DLR, and has been identified previously as a cycle of highest priority for research and development due to its potential for future realisation at an industrial scale [11] and its simple chemistry [12]. As shown in Fig. 1(b), the HyS cycle comprises two chemical reactions In the first stage, sulphuric acid is decomposed catalytically in a highly endothermic reaction at 600–1200 °C, suitable for the integration of concentrated solar thermal energy [13]. Then, the sulphur dioxide product is electrolysed together with water in the second reaction at temperatures on the order of 100 °C, requiring a minimum theoretical voltage of 0.17 V, which is only about one-seventh of the theoretical value of 1.23 V for conventional water electrolysis [14,15]. A practical and realistic efficiency of ~30% (based on the lower heating value of $H_2$) is predicted for the HyS cycle [16]. Key drivers for its development are the much lower requirement for electricity, which reduces the reliance on the relatively expensive storage of either electricity or hydrogen for continuous hydrogen production, together with the capacity to utilise low-cost thermal energy storage in the high-temperature section of the cycle [17]. In other words, one part of the electricity demand of the conventional water electrolysis is replaced by a thermal energy demand, which is much cheaper to produce and store [18,19]. The need for local storage solutions results from the large number of copper mines worldwide being located in remote areas, e. g.

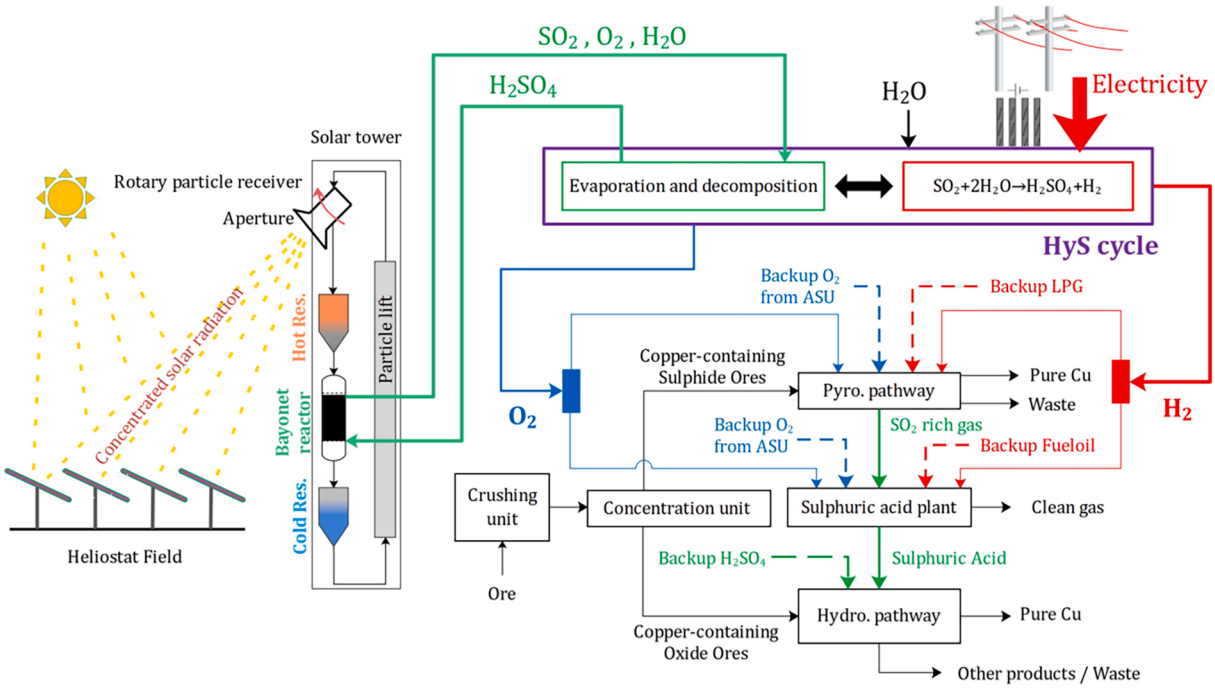


**Fig. 2.** Schematic representation of the key components of the proposed integration of the copper production plant with the HyS cycle.

Olympic Dam (OD) in Australia, Escondida Copper Mine in Chile, where solar energy is abundant, but fuel logistics can be challenging. Furthermore, there is potential to identify synergy in the sulphur cycle, with $SO_2$ being used in the HyS cycle as the circulating agent between the high-temperature sulphuric acid ($H_2SO_4$) cracking reactor and sulphur dioxide depolarised electrolyser (SDE), denoted in Fig. 1(a) as "Electrolyser", while also being a byproduct of the pyrometallurgical pathway. This can offer the potential to lower cost through compatibility of construction materials, operation, and the availability of makeup streams. A comprehensive review of the HyS cycle, reporting the main opportunities and challenges of this technology up to 2020, has been recently published by Corgnale et al. [20].

Nevertheless, to the best of the authors' knowledge, the potential benefits and challenges of integrating the HyS cycle with the copper refining process has not yet been reported. In addition no data are available of the economic potential of such integration in terms of operational expenditure (OPEX) and capital costs (CAPEX). Therefore, the objective of the current work is to assess the high-level thermodynamic potential and techno-economic feasibility of the integration of the HyS cycle and copper processing. Furthermore, the molar ratio of $H_2$ to $O_2$ in water-splitting technology is 2, while copper refineries do not necessarily require the same ratio. Therefore, the paper also aims to assess different scenarios with the view to find those with the highest techno-economic potential for the integration of the HyS cycle and copper refining process.

## 2. Description of the proposed processes

Fig. 2 presents a schematic diagram of the proposed process configuration for the integration of the HyS cycle (Fig. 1(b)) with a copper refining process (Fig. 1(a)). This potential process configuration comprises two main sections: (i) the HyS cycle and (ii) the copper processing plant. The configuration of the HyS cycle is based on the DLR's and Greenway Energy and Savannah River National Laboratory design. In this system, particles are circulated through a high-temperature solar receiver when the available concentrated solar radiation is sufficient to exceed the losses [24] and then sent to a Hot Reservoir for storage [25–27]. One plausible reactor configuration to heat the particles with concentrated solar radiation can be the rotary drum particles receiver CentRec, which has been developed and demonstrated by DLR [13,17]. Hot particles from the storage are sent to an indirectly heated Bayonet reactor to drive the endothermic splitting of sulphuric acid ($H_2SO_4$) into $SO_2$ and $O_2$ (Fig. 2) [28]. The relatively cold particles from the Bayonet reactor are then stored in a Cold Reservoir (Fig. 2) prior to re-heating. The electrolysis part of the HyS cycle is the same as the conventional HyS cycle described above [29]. Here, it is assumed that its electricity demand is to be supplied from the electrical network. The hydrogen and oxygen produced by the HyS cycle are used in the copper refining process in one of two scenarios, as follows:

1. The HyS cycle is sized to produce enough $H_2$ to meet the hydrocarbon (HC) fuel demand of the pyro pathway and sulphuric acid production plant. In this scenario, the $O_2$ product from the HyS cycle is also used in the copper refinery process, reducing the size of the ASU plant.
2. The HyS cycle is sized to meet the $O_2$ demand of the copper production process, hence mitigating the dependency on air enrichment units (such as ASU or PSA units). In Scenario 2, the $H_2$ product from the HyS cycle is also used to replace the HC fuel in the pyrometallurgy pathway and acid plant, while the excess hydrogen is given a reference value. In practice, the excess hydrogen could be used to energise some of the mine trucks, to produce electricity or be sold as revenue. It should be noted that the oxygen demand in the copper production process surpasses that of the fuel. Therefore, if the total oxygen demand is to be supplied via electrolysis, which produces 8 kg $O_2$/kg $H_2$, it will not be enough for the copper processing. Therefore, Scenario 1 also requires some oxygen to be supplied from the ASU (shown as dashed arrows in Fig. 2). However, given sufficient storage, if the HyS cycle is sized to supply the total oxygen demand of the copper plant (Scenario 2), it avoids the need for an ASU with its associated demands for energy.

Fig. 2 also shows a makeup supply of $H_2SO_4$, which is drawn as a dashed arrow. This could potentially be sourced from the outside of the plant, depending on demand. Since the extraction of metals other than copper is not considered in the current work, the amount of the required sulphuric acid depends only on the amount of the oxide-containing copper ores through the leaching and extraction process.

**Table 1**
The five copper-containing ore compositions assessed in the study.

| Ore sulphide content (wt%) | 10% | 25% | 50% | 75% | 90% |
|---|---|---|---|---|---|
| Cu (wt%) produced via pyrometallurgy | 17% | 31% | 54% | 77% | 91% |
| $CuFeS_2$ | 0.0300 | 0.0400 | 0.0500 | 0.0700 | 0.0800 |
| CuS | 0.0984 | 0.0984 | 0.0984 | 0.0984 | 0.0984 |
| $Cu_2S$ | 0.1123 | 0.4087 | 0.8823 | 1.3566 | 1.6357 |
| $Cu_2O$ | 0.9353 | 0.6288 | 0.1452 | 0.1294 | 0.0779 |
| CuO | 0.8241 | 0.8241 | 0.8241 | 0.3455 | 0.1080 |
| Sum (wt%) | 2.0000 | 2.0000 | 2.0000 | 2.0000 | 2.0000 |

## 3. Materials and methods

Previously reported models of the copper refining process are scarce. Therefore, Aspen Plus V11.0 was used to develop a comprehensive model of this process. Aspen Plus software was used because of its large property databanks, its solvers' capabilities, including their "Goal Seek" algorithms, and the ease of modification of the properties and convergence methods. The model was developed to assess the performance of the proposed process configuration for the integration of the HyS and copper refining processes (Fig. 2). It solved the governing steady-state equations of mass and energy simultaneously. The composition of the streams were calculated for the crushing unit, concentration unit, and pyrometallurgy pathway blocks via the inbuilt "SOLIDS" property package. Additionaly, through the "Customize" option in the "Properties" ribbon, the Barin's handbook [30] was addressed as the reference for the metallurgical thermodynamic calculations. The composition of the products leaving the smelter, slag cleaner, and fire refiner reactors in the pyrometallurgy pathway, were calculated using the Gibbs energy minimisation method. Due to the high degree of ionisation and high concentration of ionic species, in the HyS cycle, sulphuric acid plant and hydrometallurgy pathway blocks the ELEC-NRTL property package with ideal gas assumption was used. The "MIXED" and "CIPSD" packages were chosen as the stream class in the simulations.

The plant capacity for all simulations was assumed to be 5000 tonnes of ore/h, while the capacity factor of the concentrated solar thermal plant was varied from 0.55 to 0.75.

As a general approach in the simulation, the copper process and the HyS cycle plant were run simultaneously for each ore composition to solve (automatically) for the size of the HyS cycle (via using multiple Calculators and Design Spec units) by altering water input and circulating acid to meet the calculated demand from the copper plant.

### 3.1. Input ore composition

The input ore was assumed to comprise copper-containing and non-copper-containing minerals. The copper-containing minerals were chosen from the most common copper ores, namely chalcocite ($Cu_2S$), covellite (CuS), chalcopyrite ($CuFeS_2$), cuprite ($Cu_2O$), and tenorite (CuO). In all cases, the total mass fraction of copper-containing minerals (sulphide and oxide ores) and non-copper minerals were 2% and 98%, respectively. The five compositions considered here were labelled based on the sulphide content of the copper minerals. For example, a composition named as 10% sulphide content indicates that, within the 2% of the total copper-containing ore, the cumulative concentrations of chalcocite, covellite, and chalcopyrite are 10%, while the rest 90% accounts for the cumulative concentration of cuprite and tenorite (Table 1). The composition of non-copper containing minerals (98 wt%) was constant and included silica ($SiO_2$, 58.2 wt%), alumina ($Al_2O_3$, 10 wt%), iron (II) oxide (FeO, 25 wt%), magnesium oxide (MgO, 0.84 wt %), potassium oxide ($K_2O$, 0.8 wt%), calcium carbonate ($CaCO_3$, 3.2 wt %) and triuranium octoxide ($U_3O_8$, 0.005 wt%).

A variation in the ore's sulphide content directly impacts the amount of copper-containing ores reduced via the pyrometallurgical pathway. Table 1 reports the fraction of the copper produced via the pyrometallurgical route as a function of the inlet ore sulphide content.

### 3.2. Process flowsheet of the hybrid sulphur cycle

Fig. 3 presents the flowsheet of the HYS cycle, developed in Aspen Plus. This model has been developed from the process flow diagram reported by Niehoff et al. [16], verified against their simulations and further improved to enable: lower temperatures for the sulphuric acid

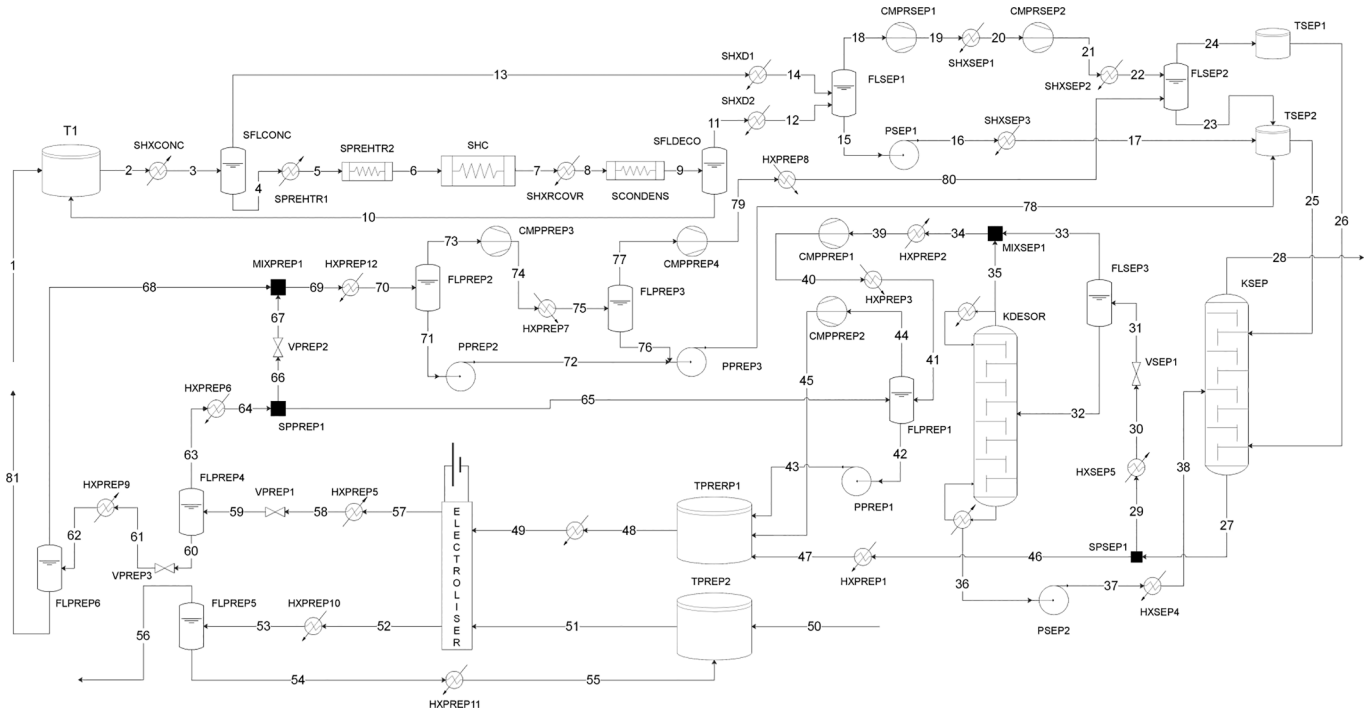


**Fig. 3.** Process flow diagram of the developed HyS cycle adapted from earlier work of Niehoff et al. (16).

**Table 2**
Comparison of the prediction of the present model of HyS with Niehoff et al.'s model (16).

| Parameter | Data from the present model | Data from Niehoff et al.'s model | Deviation (%) |
|---|---|---|---|
| Sulphuric acid concentration (wt%) | 50 | 50–75 | N/A (in range) |
| Decomposition temperature (°C) | 850 | 900–1200 | N/A (in range) |
| Hydrogen mass flow for 50 wt% acid concentration (kg/h) | 1.38 | 1.4 | 1.5% |
| Oxygen mass flow for 50 wt% acid concentration (kg/h) | 8.06 | 8.1 | 0.5% |
| Sulphuric acid mass flow (kg/h) | 98 | 98 | 0 |
| Sulphur dioxide depolarised electrolyser (SDE) efficiency | 55% | 55% | 0 |

cracking reactor and improved separation in the absorption towers Sulphuric acid makeup. This was considered to compensate for the $SO_2$ loss of the cycle. It should be noted that the HyS process was assumed to operate continuously. Therefore, the Aspen Plus simulation was carried out in the steady state condition. The full stream results of the model were compared with the model of Niehoff et al. [16] for the case with the circulating sulphuric acid concentration of 50 wt%. However, only the key indicators are reported in Table 2.

As can be seen, the differences between these two models for the hydrogen (Fig. 3, Stream 56) and oxygen mass flow (Fig. 3, Stream 28) were less than 2% for the same sulphuric acid mass flow (Fig. 3, Stream 1 and 81). The slight differences are attributable to the difference in the databases employed to estimate the thermophysical and thermochemical properties of mixtures.

The efficiency of the pumps and compressors assumed in the model was ~0.75 – 0.85, respectively [16], while that of the HyS cycle is ~25% based on the lower heating value of $H_2$ [16,29]. The hydraulic pressure losses were ignored. The ELEC-NRTL property package was used for this flowsheet. It is worth mentioning that the default ELECT-NRTL property package should be modified for a detailed study on phase separation in the KSEP absorption tower.

### 3.3. Copper refining process

The copper refining process shown in Fig. 2 includes the crushing unit, concentration unit, direct to blister smelting unit (Pyrometallurgy pathway), acid plant, and hydrometallurgy unit.

#### 3.3.1. Crushing unit process flowsheet

The process flow diagram (PFD) of the comminution and crushing plant is shown in Fig. 4. The input ore (Stream 1) is screened (SCRN-1) to remove particles smaller than 110 mm (Stream 5) from the larger particles (Stream 2, Fig. 4). A small amount of water (less than 1 wt%) is sprayed into Streams 2 and 10. The mixture (Stream 3) is sent to the first jaw crusher (JC-1). The product (Stream 4) is mixed with Stream 5 and enters the second screen (SCRN-2), from where the particles of diameter >70 mm are sent to the second jaw crusher, while the undersized particles (Stream 7) are mixed with Stream 11 (diameter ≤ 70 mm). Stream 10 recycles the particles with diameters larger than 70 mm back to the

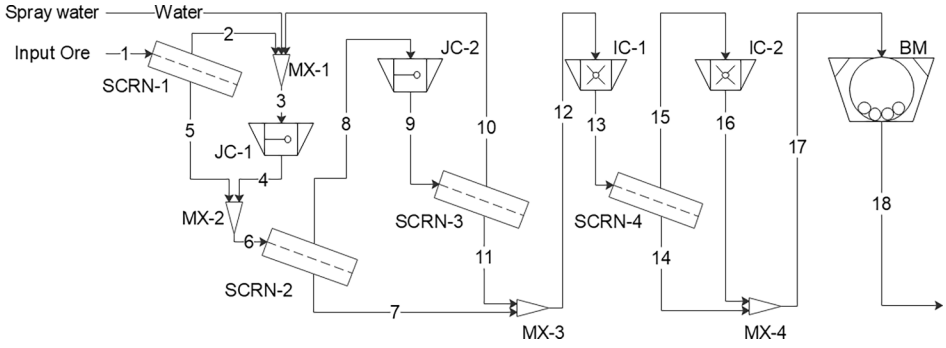


**Fig. 4.** Process flow diagram of the crushing unit.

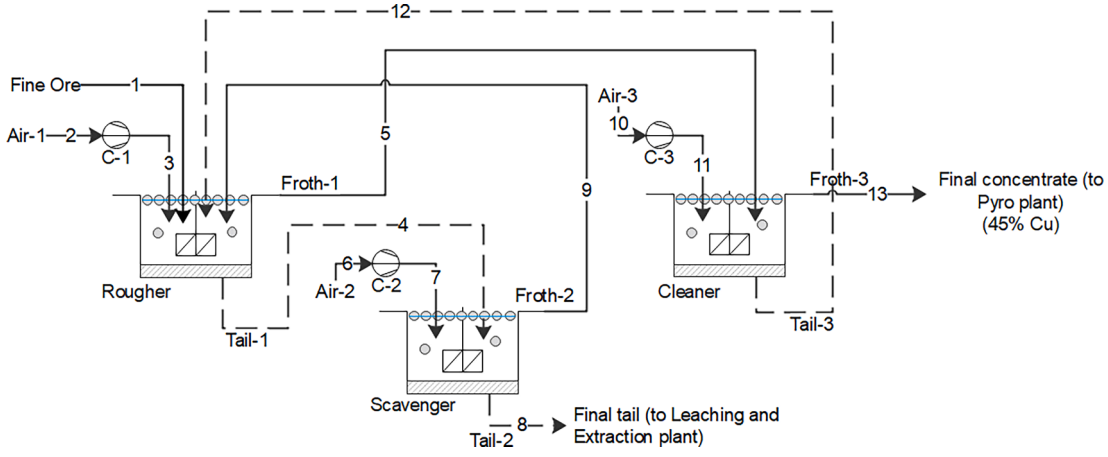


**Fig. 5.** Process flow diagram of the developed flotation unit. Stream 13, as the final froth, leaves the process with ~45% copper content, while the final tail containing other minerals, together with most of the oxide-containing copper ores, is directed to the leaching and extraction plant via Stream 8 (the final tail in Fig. 5).

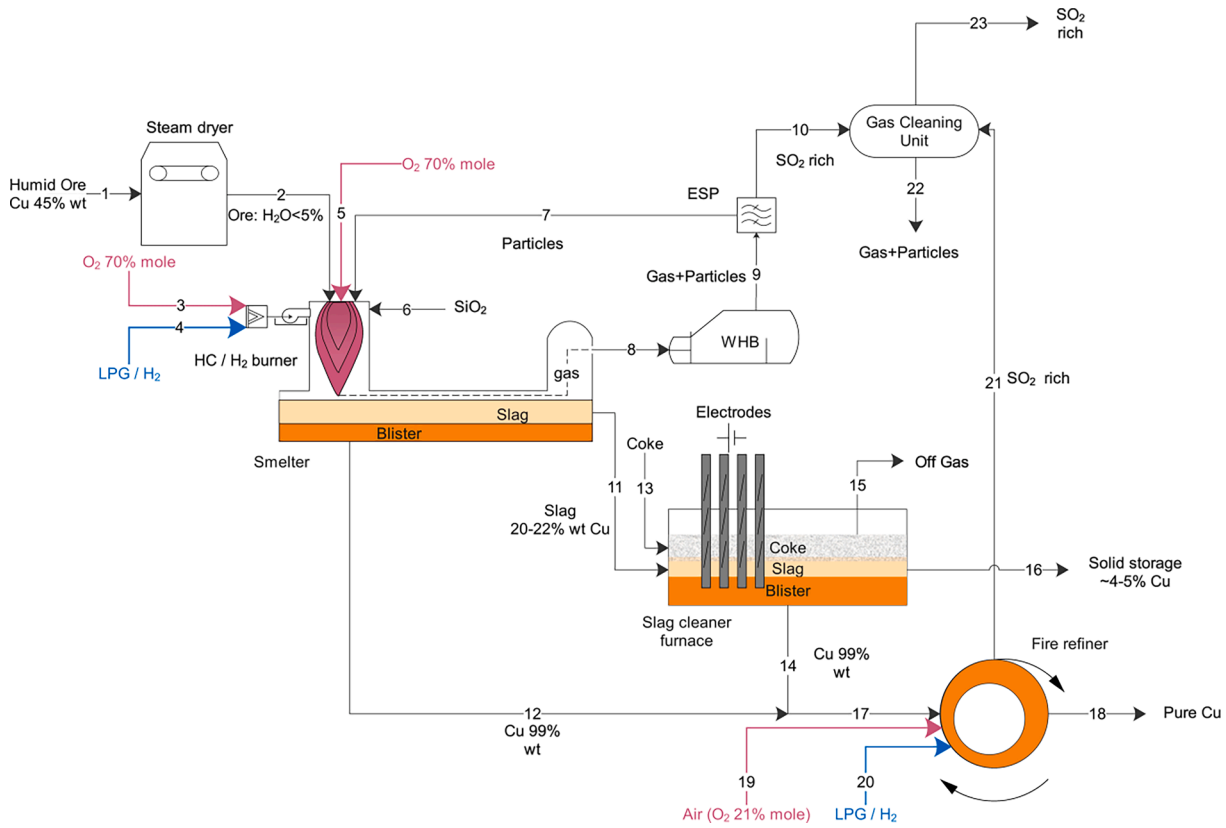


**Fig. 6.** Process flow diagram of the pyrometallurgy pathway modelled here. The blister from both the smelter and slag cleaner (Streams 12 and 14) is mixed and, after further purification in the fire refiner, refined to copper of purity >99.5 wt%. The $SO_2$-rich product gas from the smelter (Stream 10) and the fire refiner (Stream 21) is cleaned and sent to the acid plant.

first jaw crusher (JC-1). Stream 13 (diameter $\leq$ 10 mm) contains the first impact crusher (IC-1) product and is screened via SCRN4. The undersized product (Stream 14) is then mixed with the product of the second impact crusher (IC-2), Stream 16 (diameter $\leq$ 5 mm). The product (Stream 17) is sent to the ball mill (BM) and is crushed down to particles with a maximum diameter $\leq$ 100 μm [31,32].

### 3.3.2. *Concentration unit process flowsheet*

It is assumed that all the mined ores after comminution and crushing (Stream 18, Fig. 4) are sent to the flotation unit, where the oxide-containing copper ores and the sulphide-containing copper ores are mostly separated. The sulphide-containing ores are then sent to the pyrometallurgical pathway, while the oxide-containing ores and other ores are sent to the hydrometallurgical pathway. The PFD of the flotation plant modelled here is shown in Fig. 5, which includes three tanks for the separation of ores. The fine ore (diameter less than 100 μm) enters the rougher via Stream 1. Here, a fraction of the oxide and sulphide ores are separated from each other and carried via Streams 4 (as tails) and 5 (as froth). The froth from the rougher (Froth-1) enters the cleaner, where the final froth (Stream 13, Fig. 5) with an elemental Cu content of ~45% is sent to the smelters [5,7,22,33]. The tail from the cleaner (Stream 12, Fig. 5) contains some sulphide-containing ores and is sent back to the rougher. The tail from rougher (Stream 4, Fig. 5) flows to the scavenger, where the final tail (Stream 8, Fig. 5) is sent to the hydrometallurgical process. The froth leaving the scavenger (Stream 9, Fig. 5) is sent back to the rougher – the first separation step. Compressed air (P = 1.5 bar) is used to float sulphide-containing copper ores from the mixture in the tanks.

### 3.3.3. *Pyrometallurgy unit process flowsheet (direct to blister method)*

Moist ore from the concentration unit (Stream 13, Fig. 5) is sent with the particles of Cu ~45 wt% to the pyrometallurgical pathway, which comprises mostly of smelters, a slag cleaner and fire refiner. First, the water content of the ore is decreased using a steam dryer at ~T = 200 °C to final ore moisture (Stream 2, Fig. 6) of ~5 wt%. The dried ores, the flux with 98 wt% silica and the recycled particles (Stream 2, 6 and 7, respectively) are mixed and added to the smelter reaction shaft. An oxygen-enriched stream (Stream 5) is also injected into the smelter through tuyers to oxidise the sulphur content of the ore to $SO_2$. The heat duty of the smelter is supplied from the combustion of a fuel (a hydrocarbon or hydrogen, Stream 4, Fig. 5) with oxygen (Stream 3, Fig. 5) in the reaction shaft. An ASU unit supplies the required oxygen. The products of the combustion in the flue gas are mixed with the gases released during the metallurgical processes, mainly $SO_2$, and therefore contains a large amount of $SO_2$. Some 8–15% of the inlet particles are also carried with the smelter off-gas (Stream 8, Fig. 6), which are then cooled down to ~500 °C in the waste heat boiler (WHB) and are sent to an electrostatic precipitator (ESP), where the entrained particles are separated and recycled back to the smelter (Stream 7, Fig. 6), while the $SO_2$-rich gas (Stream 10, Fig. 6) is sent to the gas cleaning unit. The ore in the smelter reactor melts and is carried to either the slag or blister stream, based on its density. The slag and blister contain ~20–22 wt% and ~95–99 wt% copper, respectively. The slag is sent to the slag cleaner furnace via Stream 11, Fig. 6, where a layer of coke covers the molten mixture (to prevent the oxidation of molten metal with the ambient air), and electricity is applied to purify the molten mixture further. The slag leaving the slag cleaner (Stream 16, Fig. 6) contains ~4–5 wt% Cu and is typically discarded or stored for recycling. The off-gas from the slag cleaner contains mostly carbon dioxide resulting from reacting the coke with the oxygen released from the metal ores during the reduction process. The present study does not consider the substitution of coke with hydrogen; however, one could consider such

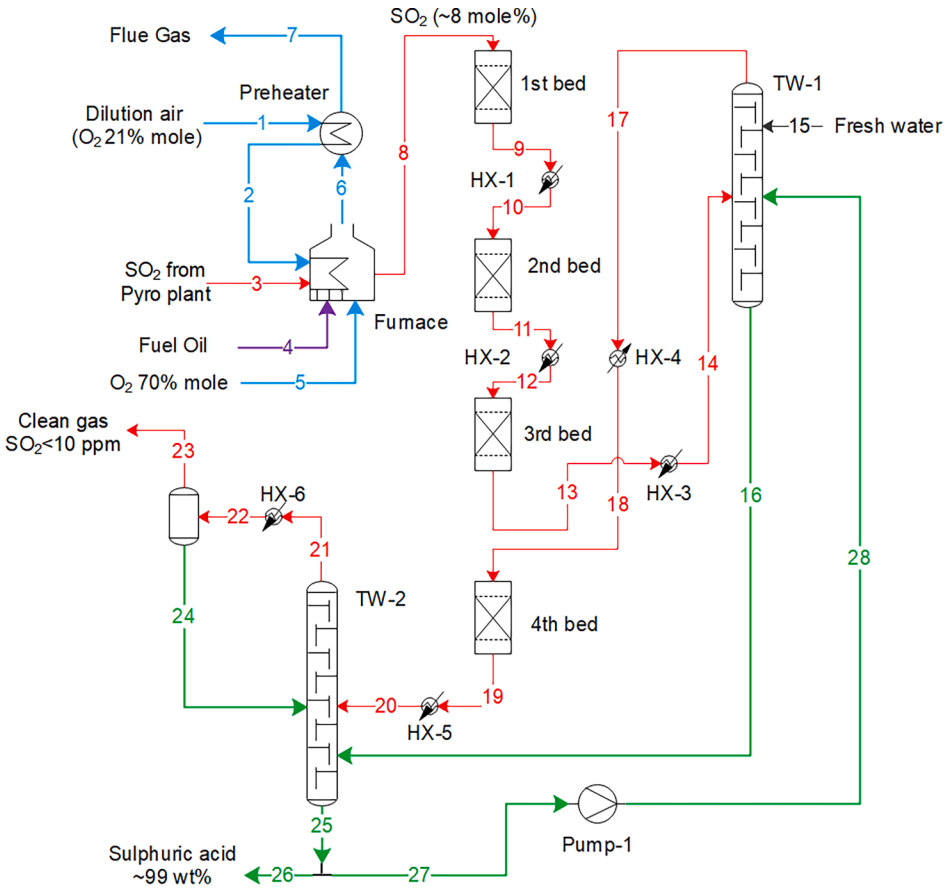


**Fig. 7.** Process flow diagram of the developed acid plant. The sulphuric acid product concentration is ~99 wt%, while the clean gas leaving the plant has less than 10 ppm $SO_2$.

replacement as a subsequent step if the reactor were to operate under a neutral atmosphere, such as Argon.

The blister leaving the smelter and the slag cleaner (Stream 12 and 14) is sent to the fire refiner reactor, where fuel and air are used to increase the copper purity to more than ~99.5 wt%. The temperature of the smelter and the slag cleaner are ~1300 °C and ~1310 °C, respectively [7,33–35]. Here, it is assumed that Stream 23 contains mostly sulphur dioxide ($SO_2$), nitrogen ($N_2$), and oxygen ($O_2$). Stream 23 in Fig. 6, with a temperature of < ~100 °C, is sent to the acid plant unit, where the $SO_2$ is converted to sulphuric acid [7].

To account for the smelter duty, while maintaining the smelter temperature at ~1310 °C, the Aspen Plus RGIBBS reactor package was used to model the combustion of LPG with oxygen-enriched air. The flame generates product gases at 1320 °C and 1 bar after the heat has been transferred to the smelter reactor. It is assumed that ~50% of the generated heat from combusting LPG with enriched air is used to maintain the temperature of the streams at 1300 °C throughout the pyrometallurgical copper production. Finally, the flow rate of the oxygen (Stream 5 in Fig. 6) is matched to ensure that the concentration of $Cu_2S$ in the smelter is always <0.2 wt% to minimise foaming [5,7,36,37]. The effect of oxygen flow rate on the product composition is shown in Fig. 10. It is worth mentioning that the RGIBBS package with phase and product specification was used to model the smelter, the slag cleaner and the fire refiner products.

### 3.3.4. Acid plant flowsheet

Fig. 7 shows the flowsheet of the acid plant that was modelled here, which incorporates two absorption columns and a four-stage catalytic bed reactor [38]. A stream of air (Stream 1) is preheated and mixed with the $SO_2$-rich stream coming from the pyrometallurgical pathway (Stream 23, Fig. 6) to lower the $SO_2$ concentration to ~8 mol% (Stream 8). Fuel oil (Stream 4) is burnt with an oxygen-rich stream (Stream 5) to supply the required heat. The exothermic conversion of $SO_2$ to sulphur trioxide ($SO_3$) occurs in the catalytic bed reactors (the "1st bed" to the "4th bed"). It should be noted that the gas mixture temperature after each catalytic conversion step is decreased to ~400 °C to optimise the $SO_2$ oxidation reaction [38,39]. The mixture leaving the "3rd bed" (Stream 13 with $SO_2$ < 0.0008 mol%) is cooled and sent to the first absorption tower (TW-1). Freshwater (Stream 15) and concentrated sulphuric acid (Stream 28) are fed to the TW-1 to absorb the $SO_3$ product using a circulating concentrated sulphuric acid solution.

The top product of TW-1 is sent to the last catalytic bed (Stream 18, Fig. 7), while the bottom product (Stream 16) is fed to the second absorption tower, "TW-2″, where the remaining $SO_3$ is absorbed from the cooled gas mixture leaving from the last catalytic bed (Stream 20). The gas leaving from TW-2 (Stream 21) is cooled to condense and recycle the sulphuric acid vapour via stream 24. The mole fractions of $SO_2$ and $SO_3$ in the final gas leaving the process (Stream 23) are ~5 and ~1 ppm, respectively. Both TW-1 and TW-2 have five equilibrium stages for the production of $H_2SO_4$ from $SO_3$ and $H_2O$ and a pressure of 1.2 bar at their top.

A pump-around flow is assumed for each tower to recycle the liquid from the bottom to the top stages, although this is not shown in Fig. 7 for clarity. The required flow of the pump-around stream depends on the $SO_2$ content of the pyrometallurgy pathway gases.

A fraction of the acid product with a ~99 wt% acid content (Stream 26, Fig. 7) is sent to the hydrometallurgy process for the leaching process, depending on the ore composition. For the assessment here, it is assumed that the extra sulphuric acid required for this step is shipped to the site if the sulphuric acid produced in the acid plant is insufficient to

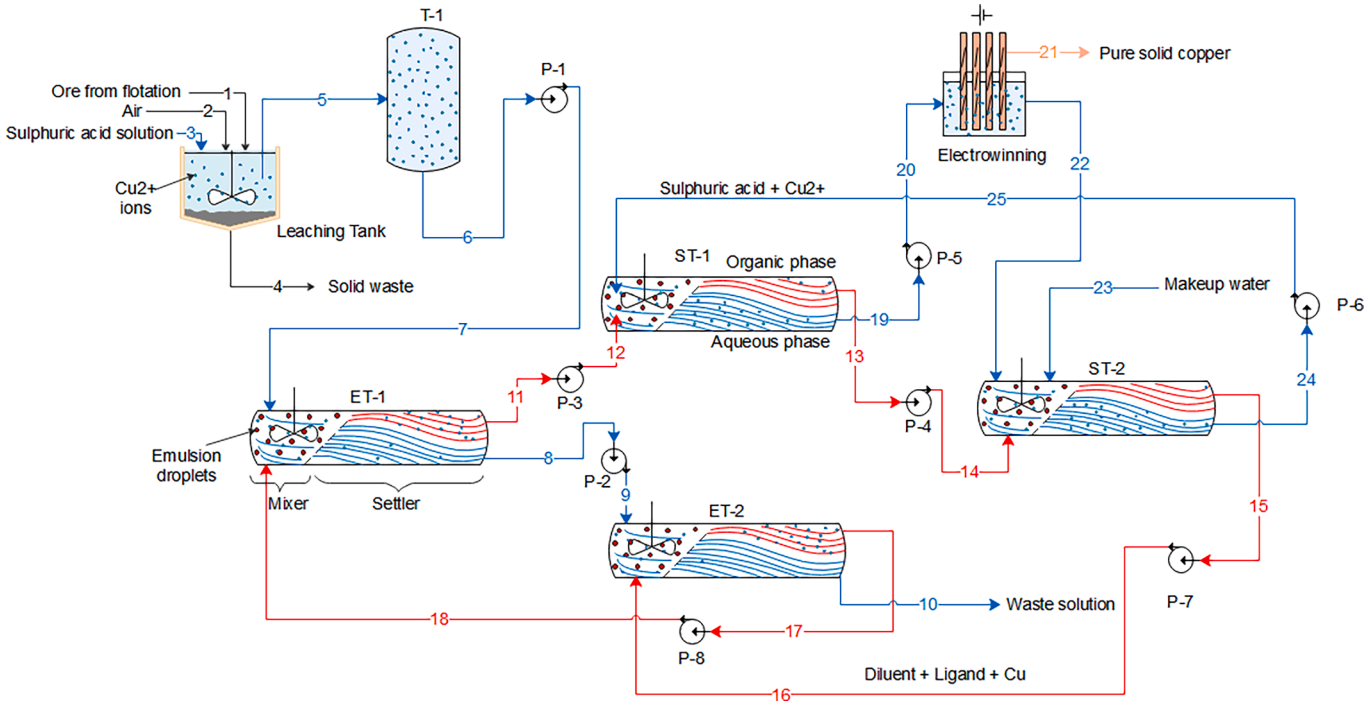


**Fig. 8.** Process flow diagram of the hydrometallurgy pathway evaluated here. The ore is leached in a leaching tank and then fed to the solvent extraction cycle, which comprises two extraction tanks (ET-1 and ET-2) and two stripping tanks (ST-1 and ST-2). Next, the copper ions are removed in Stripping Tanks ST-1, and ST-2 and the solution is sent to the electrowinning reactor, which deposits pure copper using electricity.

meet this demand.

### 3.3.5. *Hydrometallurgy flowsheet*

A schematic representation of the hydrometallurgical pathway process is depicted in Fig. 8. The main sections of the plant are those of acid dissolution, solvent extraction and electrowinning. In the acid dissolution (i.e. leaching) section, the Flotation tail, air and the sulphuric acid solution (Streams 1, 2 and 3, respectively) are mixed in the leaching tanks, where the sulphuric acid dissolves the copper oxide, cupric oxide and other metallic compounds in the ore, following which the supernatant is sent to T-1. The solvent extraction comprises two extraction tanks (ET1 and ET2) and two stripping tanks (ST-1 and ST-2) [6,40,41]. The acidic solution containing the copper ions (Stream 6, Fig. 8) is pumped to the first extraction tank (ET-1), where an organic phase containing kerosene as the diluent and a ligand (LH) is mixed with it to extract the copper ions in the form of $L_2Cu$ [6,42]. This also lowers the pH of the aqueous solution. The aqueous phase leaving the first extraction tank is transferred to ET-2, where the organic phase absorbs the remaining copper ions in the aqueous solution. The outlet stream from the second extraction stage (Stream 10) contains ~300 ppm $Cu^{2+}$. To purify the solution further, the stripped organic phase leaving ST-2 (Stream 15) is sent to the ET-2, where more copper ions are separated. The organic phase from ET-2 is not saturated with copper ions and hence is sent to the ET-1 to further extract $Cu^{2+}$ ions from the aqueous phase. The loaded organic phase is next stripped of copper ions in ST-1 and ST-2 using a cycling acid solution, after which they are deposited in an electrowinning reactor. Since some water is consumed in the electrowinning reactor, a water makeup stream is added to ST-2 (Stream 23,

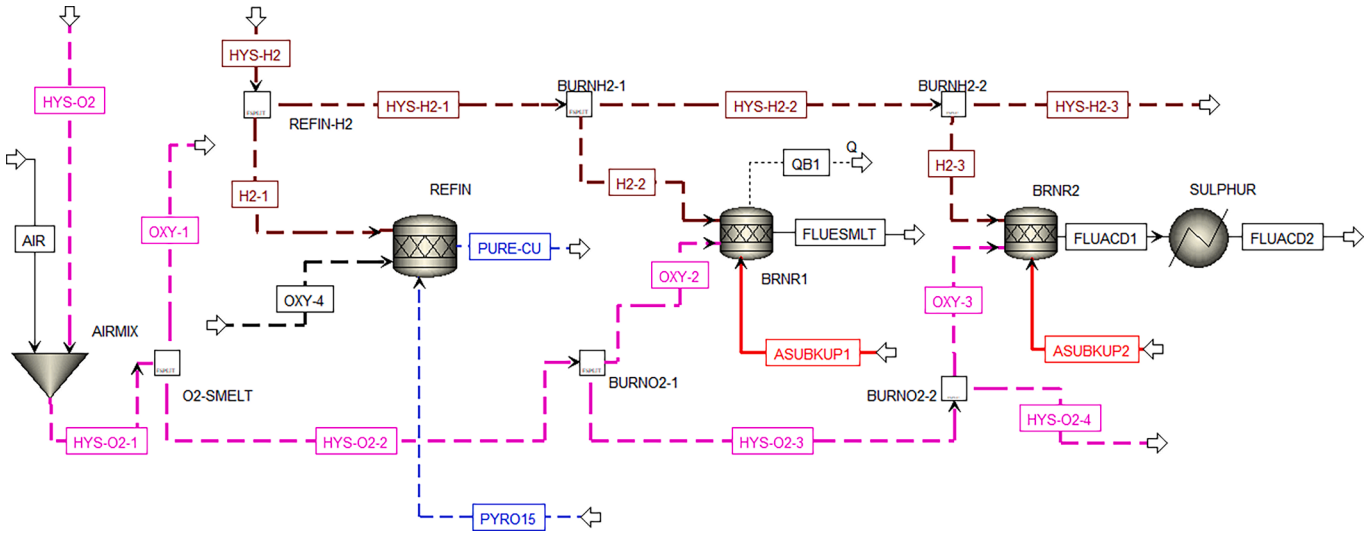


**Fig. 9.** The points in the copper production cycle where the outputs from the HyS cycle are used in the copper production plant via scenarios 1 and 2.

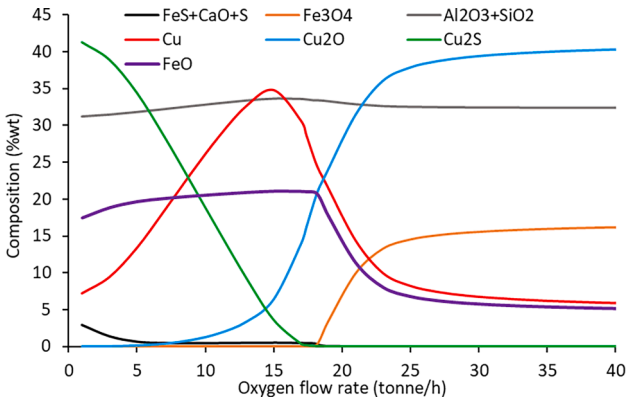


**Fig. 10.** The effect of oxygen flow rate through the tuyeres on the smelter product composition at 1300 °C and 1 bar, as calculated with the model.

Fig. 8). Some pH balancing and neutralisation of Stream 10 may then be required before being discharged into the environment, which is not shown in Fig. 8.

While some further solvent extraction cycles may be employed in practice to dissolve small amounts of uranium, gold and/or silver [41,43], these are ignored here. This simplification follows earlier work [43,44].

### 3.4. Integration of the hybrid sulphur cycle with the copper production plant

The HyS cycle (Fig. 3) was reproduced from Niehoff et al. [16], with an efficiency that is a function of both decomposer temperature and circulating sulphuric acid concentration. For a decomposer temperature of 850 °C and circulating sulphuric acid concentration of 50 wt%, the HyS cycle efficiency varies between 18 and 25% for cases without and with heat recovery, respectively.

Fig. 9 presents the approach evaluated with which the HyS cycle is integrated with the copper production cycle. The $H_2$ and $O_2$ products from the HyS cycle are sent to the copper production cycle via streams HYS-H2 and HYS-O2, respectively. A small fraction of the hydrogen (Stream H2-1) is sent to the refiner reactor (REFIN) to reduce the oxides. In addition, ambient air (21 mol% oxygen) is supplied to the reactor via OXY-4.

The oxygen product of the HyS cycle (HYS-O2) contained ~99 mol% oxygen and was diluted with the ambient air (AIR) to get ~70 mol% oxygen content in the HYS-O2-1 stream before being fed to the smelter via the OXY-1 stream in Fig. 9 (the equivalent of Stream 5 in Fig. 6).

The smelter duty was also supplied by burning the oxygen-rich stream (OXY-2) with the hydrogen stream (H2-2) in the BRNR1 burner. For Scenario 1, where the oxygen product from the HyS cycle would not be sufficient to cover all the demands, makeup oxygen from the ASU units are utilised (ASUBKUP1 and ASUBKUP2 streams).

H2-3, OXY-3 and ASUBKUP2 streams in Fig. 9 provided the required duty for the second burner (BRNR2) located in the acid plant (Furnace in Fig. 7) and replaced the fuel oil with hydrogen. The "SULPHUR" heater in Fig. 9 represents the total exchanged heat from the flue gas to the SO2-rich stream (combined duties of furnace and preheater in Fig. 7). The flow rate of HYS-H2-3 stream is zero in Scenario 1. However, in Scenario 2, since the HyS cycle is sized to produce the required oxygen for the process, extra hydrogen would be produced, and the flow rate of the HYS-H2-3 stream will not be zero. It should be noted that since the HyS cycle would operate only when enough solar or stored thermal energy is available, its hydrogen and oxygen production is prone to intermittency and therefore, capacity factors should be considered (CF: 0.55 to 0.75).

## 4. Results and discussion

In Section 4.1, the results specific to the modelled copper plant are discussed. Then in Section 4.2, the results for the integration of the HyS cycle with copper refiner are reviewed. Sections 4.3 and 4.4 discuss the potential $CO_2$ reduction and the economics of the integration via both scenarios.

### 4.1. Copper production plant

Table 3 presents the assumed particle size distribution (PSD) of the input ore stream (Stream 1, Fig. 4), together with the calculated PSD in each successive stream within the comminution and crushing processes (Fig. 4). Also shown are the solids flow rate and the calculated specific energy for each size reduction stage. A constant grindability of 12 kWh / tonne of solid was assumed for the Bond work index, following earlier works [31,45,46].

The results from Table 3 are consistent with the expectation that the specific energy for comminution increases with a reduction in the particle diameter. The crushing unit requires ~81.75 MJ/tonne of solids to reduce the particle size distribution to less than or equal to 100 μm without considering the conveying and screening energy.

Table 4 reports the calculated values of the flow rate and composition of the final froth (feed to the pyrometallurgical pathways) and tail (feed to the hydrometallurgical pathways) in the flotation unit (Fig. 5) on a dry basis for various values of ore composition. The flow rates and the separation ratios of each component in the rougher, scavenger and cleaner units were adjusted for each composition to assure that the stream leaving the flotation to smelter contains ~45 wt% elemental copper [7,35].

Returning to Fig. 6, which presents the pyrometallurgy pathway, it can be seen that the moist ore (final froth from the flotation unit) is dried

**Table 3**
The particle size distributions, both of the input ore (assumed) and as calculated after each comminution step, together with the values of specific power determined with the model.

| Stream No. (Fig. 4) Particle Size Distribution | 1 | 4 | 9 | 13 | 16 | 18 |
|---|---|---|---|---|---|---|
| 0–20 μm | 0 | 0.012 | 0.020 | 0.034 | 0.083 | 0.045 |
| 20–100 μm | 0 | 0.002 | 0.004 | 0.059 | 0.100 | 0.955 |
| 100–300 μm | 0 | 0.002 | 0.003 | 0.126 | 0.172 | 0 |
| 300–1000 μm | 0 | 0.002 | 0.004 | 0.299 | 0.624 | 0 |
| 1000–5000 μm | 0 | 0.005 | 0.009 | 0.443 | 0.022 | 0 |
| 5000–10,000 μm | 0.05 | 0.008 | 0.019 | 0.039 | 0 | 0 |
| 10,000–20,000 μm | 0.10 | 0.064 | 0.203 | 0 | 0 | 0 |
| 20,000–70,000 μm | 0.55 | 0.328 | 0.735 | 0 | 0 | 0 |
| 70,000–110,000 μm | 0.10 | 0.576 | 0.004 | 0 | 0 | 0 |
| 110,000–150,000 μm | 0.20 | 0.001 | 0 | 0 | 0 | 0 |
| Equipment in simulation | NA | JC-1 | JC-2 | IC-1 | IC-2 | BM |
| Type of Crushing / Grinding | NA | Jaw Crusher | Jaw Crusher | Impact crusher | Impact crusher | Ball mill |
| Solid flow rate (tonne /h) | 5000 | 1622 | 1047 | 5000 | 2126 | 5000 |
| Specific Energy (MJ / tonne solid) | NA | 0.25 | 0.68 | 5.99 | 13.01 | 70 |

**Table 4**
Calculated values derived with the model of the flow rates and composition of the final froth and final tail, leaving the concentration unit in the flotation circuit for various values of sulphide content in the ore.

| Ore sulphide content (wt %) | 10% | | 25% | | 50% | | 75% | | 90% | |
|---|---|---|---|---|---|---|---|---|---|---|
| Cu (wt %) produced via pyrometallurgy | 17% | | 31% | | 54% | | 77% | | 91% | |
| Outlet type | Froth | Tail | Froth | Tail | Froth | Tail | Froth | Tail | Froth | Tail |
| Mass flow rate (tonne / h) | 30 | 4970 | 54 | 4946 | 93 | 4907 | 132 | 4868 | 156 | 4844 |
| Elemental Cu (wt %) | 45.03 | 1.39 | 45.2 | 1.10 | 45.10 | 0.75 | 45.20 | 0.38 | 45.03 | 0.15 |
| Component (wt %) | | | | | | | | | | |
| Silica ($SiO_2$) | 10.36 | 58.44 | 14.33 | 58.64 | 17.48 | 58.93 | 21.05 | 59.16 | 18.03 | 59.45 |
| Alumina (Al2O3) | 1.78 | 10.05 | 1.97 | 10.09 | 2.86 | 10.14 | 3.82 | 10.17 | 3.07 | 10.22 |
| Iron (II) oxide (FeO) | 27.13 | 24.99 | 23.96 | 25.01 | 20.83 | 25.08 | 16.37 | 25.23 | 20.53 | 25.14 |
| Magnesium oxide (MgO) | 0.00 | 0.85 | 0.00 | 0.85 | 0.00 | 0.86 | 0.00 | 0.86 | 0.00 | 0.87 |
| Potassium oxide (K2O) | 0.00 | 0.80 | 0.00 | 0.81 | 0.00 | 0.82 | 0.00 | 0.82 | 0.00 | 0.83 |
| Calcium carbonate (CaCO3) | 0.00 | 3.22 | 0.00 | 3.24 | 0.00 | 3.26 | 0.00 | 3.29 | 0.00 | 3.30 |
| Triuranium octoxide (U3O8) | 0.00 | 0.01 | 0.00 | 0.01 | 0.00 | 0.01 | 0.00 | 0.01 | 0.00 | 0.01 |
| Chalcopyrite (CuFeS2) | 4.97 | 0.00 | 3.67 | 0.00 | 2.67 | 0.00 | 2.64 | 0.00 | 2.56 | 0.00 |
| Covellite (CuS) | 16.30 | 0.00 | 9.03 | 0.00 | 5.26 | 0.00 | 3.71 | 0.00 | 3.14 | 0.00 |
| Chalcocite (Cu2S) | 18.59 | 0.00 | 37.49 | 0.00 | 47.17 | 0.00 | 51.13 | 0.00 | 52.25 | 0.00 |
| Cuprite (Cu2O) | 11.09 | 0.87 | 4.13 | 0.59 | 0.56 | 0.14 | 0.35 | 0.12 | 0.18 | 0.07 |
| Tenorite (CuO) | 9.77 | 0.77 | 5.42 | 0.77 | 3.16 | 0.78 | 0.93 | 0.33 | 0.25 | 0.10 |

**Table 5**
Simulated values of the contribution to copper recovery from each of the various stages in the process for a series of values of ore compositions.

| Component wt% Sulphide content | 10% | 25% | 50% | 75% | 90% |
|---|---|---|---|---|---|
| Cu wt% produced via pyrometallurgy | 17% | 31% | 54% | 77% | 91% |
| Cu wt% produced via hydrometallurgy | 83% | 69% | 46% | 23% | 9% |
| Cu wt% content in the slag | 21.9% | 20.8% | 20.6% | 20.8% | 20.5% |
| Cu wt% content in the discarded solids | 5.6% | 5.4% | 5.4% | 5.5% | 5.4% |
| Yield (Cu in / Cu out) | 89.7% | 90.3% | 91.2% | 92.2% | 92.7% |

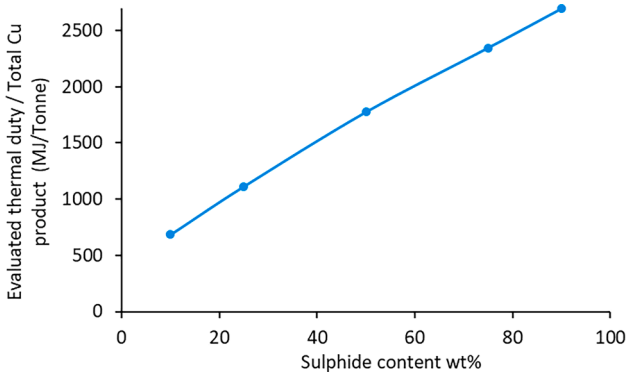


**Fig. 11.** Effect of copper ore sulphide content on the estimated total thermal duty of the pyrometallurgical pathway, as calculated with the model.

with superheated steam to recover energy [7]. The required mass flow rate of steam was estimated to be ~1.1 times more than that of the ore. The semi-dried ore has a temperature of ~130 °C, moisture content of less than 3 wt% and a mass flow rate of ~15% of the smelter input ore mass flow rate. The flux contains quick lime (CaO, 2 wt%) and silica ($SiO_2$, 98 wt%). The slag (20–22 wt% Cu) is separated from the matte by density difference and introduced to the slag cleaner for further purification. The slag stream leaves the slag cleaner with ~5–7 wt% Cu. The calculated values of Cu wt% in the slag and the discarded solids are shown in Table 5 for the various values of ore compositions and the copper yield (i.e. the ratio of Cu at the inlet to the outlet).

Fig. 10 presents the dependence of the smelter product composition on the oxygen flow rate through the tuyeres (Fig. 6), calculated with the

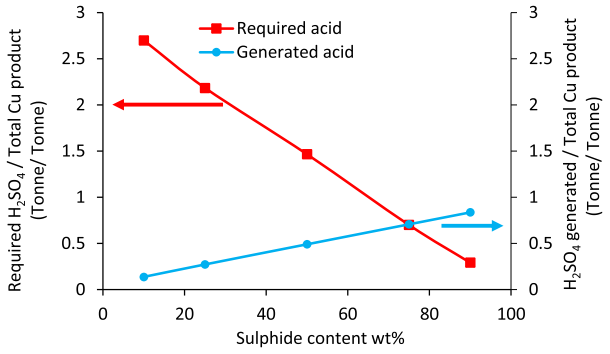


**Fig. 12.** Effect of copper ore sulphide content on the amount of sulphuric acid required for leaching per tonne of copper product, together with the corresponding effect on the amount of sulphuric acid produced.

Gibbs reactor at ~1310 °C and 1 bar for the case of sulphide content equal to 50 wt%. Although the maximum Cu yield can be obtained with an oxygen flow rate of ~15 tonnes/h, the concentration of $Cu_2S$ should be kept below 0.2 (wt%) to avoid foaming in the smelter [7,47]. Hence the oxygen flow rate chosen for operation is ~17.42 tonne/h.

Fig. 11 presents the estimated thermal duty of the pyrometallurgy flowsheet per tonne of copper as a function of sulphide content in the ore. It can be seen that an increase in the sulphide-containing fraction of copper ore results in an increase in required thermal duty. These results are influenced by the requirement to use (chemically neutral) flux, which prevents auto-thermal conditions from being reached with an increase in the sulphur content. This maintains the Cu concentration constant at ~40 wt% in the feed. The effect of an increase in the exothermic reduction of copper with an increase in the sulphide content of the ore was observed in the available heat from the waste heat boiler (WHB), as the primary heat recovery unit. For ore compositions of 10 to 90 wt% sulphide content, the duty ratio of waste heat boiler (WHB) to the smelter spanned ~85 to 104%, respectively.

The total heat loss in the pyrometallurgical flowsheet was assumed to be ~50% of the combusted fuel. In addition, it is assumed that ~10% of the heat is carried out from the smelter by the particles in the gaseous stream. These particles are sent back to the smelter after passing through the WHB and electrostatic precipitator (ESP) (Fig. 6). Therefore, only a fraction of the particles sensible energy can be recovered.

Fig. 12 presents the amount of acid generated per tonne of copper product (blue circles) as a function of sulphur content (Fig. 7). These were calculated assuming that the pH of the effluent stream leaving the

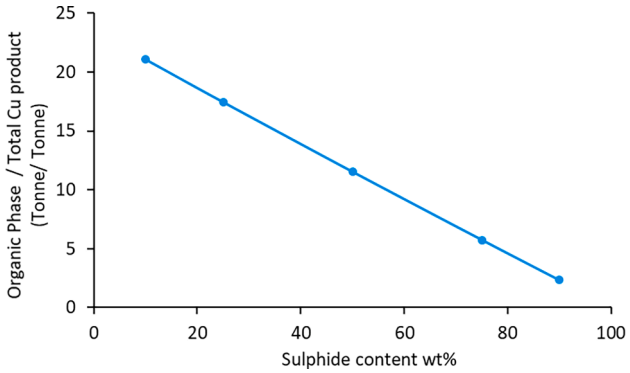


**Fig. 13.** Effect of copper ore sulphide content on the flow rate of circulated organic phase per tonne of copper product.

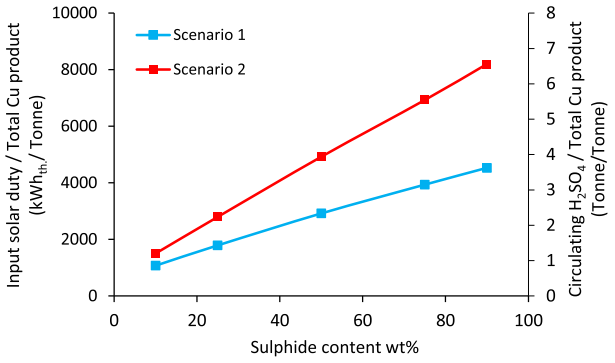


**Fig. 14.** Effect of copper ore sulphide content on the required solar input and the circulating sulphuric acid (in the HyS cycle) for scenarios 1 and 2, as calculated with the model.

leaching tanks (Stream 5 in Fig. 8) was ~0.8. It can be seen that this production rate increases with an increase in the ore sulphur content. As mentioned in the section describing the hydrometallurgy flowsheet, the flotation tail containing the copper oxide ores, together with other minerals such as silica, alumina and iron oxide (II), is sent to leaching tanks where the copper oxide ores are dissolved with the aid of the sulphuric acid solution and air. The amount of acid required can also be seen to be a function of the ore composition (red squares). More specifically, an increase in the sulphide content of the ore leads to a decrease in the amount of acid required for the leaching. Hence, for ores with 10, 25 and 50 wt% sulphide content, an acid makeup stream is necessary to fully dissolve the copper oxide ores. However, for cases of 90 wt% sulphide content, the acid produced in the acid plant is more than sufficient to provide the acid for the leaching tanks. The critical value of sulphide content for which the acid requirements equal that produced is approximately 75%.

The effect of sulphide content on the circulating organic phase mass flow rate is depicted in Fig. 13 for the organic solution containing 50 wt % ligands and 50 wt% organic diluents (e.g. kerosene), which was used to extract the dissolved $Cu^{2+}$ from the effluent stream. The final stream contained ~300 ppm (weight basis) $Cu^{2+}$ ions. An increase in the ore sulphide content can be seen to decrease the dependence of the copper refining on the hydrometallurgical pathway, reducing its load and decreasing the requirement for a circulated organic phase to strip the copper ions.

### 4.2. The hybrid sulphur cycle and its integration with copper refinery

Fig. 14 presents the calculated solar input required to evaporate the sulphuric acid and decompose it to $SO_2$, $O_2$ and water for each of the two

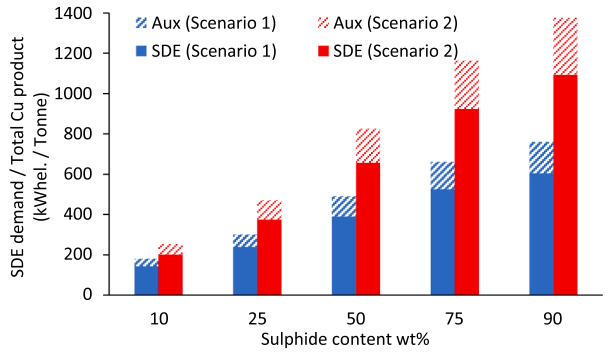


**Fig. 15.** Effect of copper ore sulphur-content on the required electricity in the HyS cycle for scenarios 1 and 2.

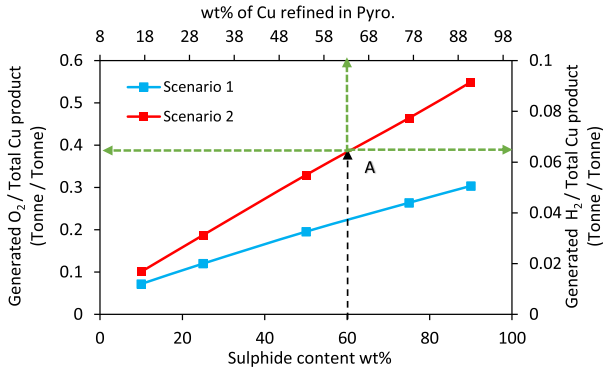


**Fig. 16.** Effect of copper ore sulphur-content and fraction of copper produced in the pyro furnaces on the amount of $H_2$ and $O_2$ required to be produced with the HyS cycle for scenarios 1 and 2.

scenarios, together with the required flow rate of circulated $H_2SO_4$ solution (50 wt%) per tonne of Cu product. It can be seen that an increase in the sulphur content of the ore leads to an increase in the input solar duty and circulated $H_2SO_4$. In addition, since the oxygen demand from the copper production process is higher than the hydrogen demand, the size of the HyS cycle for Scenario 2 is greater than for Scenario 1.

Fig. 15 presents the electrical energy required for the $SO_2$ depolarised electrolyser (SDE) used to recombine $SO_2$, $O_2$ and $H_2O$ to the sulphuric acid (Fig. 2) as a function of the sulphide content of the ore for both scenarios. It can be seen that the required electrical duty for SDE increases with sulphide content up to a maximum value of approximately 1.2 $MWh_e/t_{Cu}$, which corresponds to 115 kJ/mole $SO_2$. The auxiliary power needed to circulate the fluids via pumps and compressors is also shown. This is approximately one-quarter of the demand of the SDE.

The hydrogen and oxygen production rate from the HyS cycle is presented in Fig. 16 as a function of sulphide content in the ore for the two scenarios. Also shown on the secondary abscissa is the fraction of the copper ore that is processed via pyrometallurgy (the equivalent of the 2nd row in Table 4). Point A in the Fig. 16 represents the example of the case for which the sulphur content of the ore is 60%, for which the corresponding fraction of the ore refined in the pyrometallurgical pathway is ~64% if the plant is integrated with the HyS cycle via Scenario 2. For this case, the HyS cycle also provides ~0.39 tonnes of oxygen and ~0.062 tonnes of hydrogen per tonne of Cu. Since the pyro pathway only requires ~0.039 tonnes of hydrogen, the residual (0.023 tonnes) is the excess hydrogen. The molar purities of the oxygen and hydrogen streams shown in Fig. 16 are also calculated to be 0.99 and 0.96, respectively.

Fig. 17 presents the requirements calculated with the model for

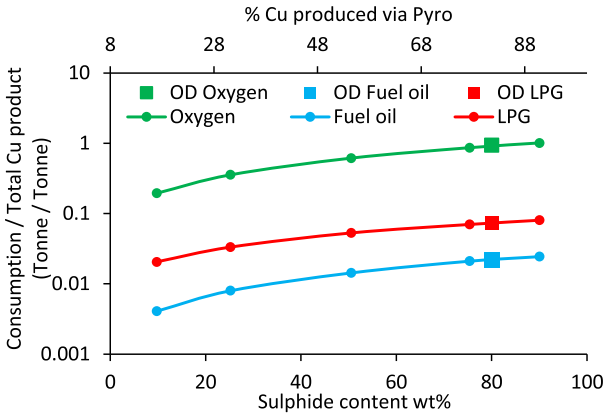


**Fig. 17.** Effect of copper ore sulphur-content and the fraction of copper production in the pyro furnaces on the consumption of oxygen, LPG and fuel oil. The square symbols are the published consumption of these inputs by the BHP copper production plant at Olympic Dam (OD) Australia (44).

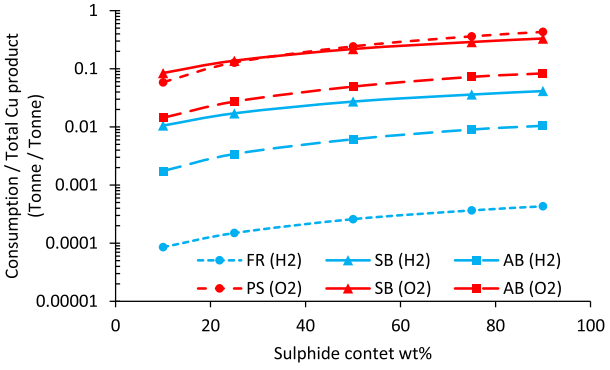


**Fig. 18.** Effect of sulphur-content of the copper ore on the $H_2$ and $O_2$ demands from the pyro furnaces for the case in which these gases are supplied from the HyS cycle. Here the terms FR, AB, SB and PS are fire refiner, acid plant burner, smelter burner and process smelter, respectively.

oxygen, LPG and fuel oil per tonne of Cu for the reference case for which fossil fuel is used to provide the energy as a function of sulphide content of the ore. Also shown on the secondary axis is the fraction of copper that is produced via the pyrometallurgical pathway and the corresponding published consumptions of the operating copper plant of BHP's plant at the Olympic Dam (OD) site in Australia [33,36,44]. Consistent with Figs. 11 and 16, the consumption of both fuels and of oxygen increases with the sulphide content of the ore, as does the fraction of copper produced via the pyrometallurgical pathway. Note that, even for the case for which the inlet ore comprises only sulphides, some 10–20% of the copper is still produced via the hydrometallurgical pathway, and only the rest is produced via the pyrometallurgical pathway. This is because the uranium content of this ore is removed by leaching with sulphuric acid, which also dissolves, ~10–20% of the copper that is recovered via the hydrometallurgical pathway.

Fig. 18 presents the corresponding amounts of hydrogen and oxygen required by the copper production plant to avoid consuming both hydrocarbon fuels and some, or all, of the oxygen demand, which is conventionally supplied with air separation units (ASU) via scenarios 1 and 2, respectively. Here the acronyms FR, AB, SB and PS correspond to the fire refiner (Fire refiner in Fig. 6), acid plant burner (Furnace in Fig. 7), smelter burner (HC/$H_2$ Burner in Fig. 6) and the process smelter (Stream 5 in Fig. 6), respectively. It is evident that the main consumer of $H_2$ is the smelter burner. However, for $O_2$, the primary consumers are the smelter burner and the oxygen that is used in the reduction reactions of copper.

The total $O_2$ demand from the copper plant for Scenario 2 is the sum of the PS, SB, and AB requirements. A comparison between Figs. 17 and 18 shows that the copper production plant would consume slightly less oxygen if $H_2$ was used as fuel rather than hydrocarbons. This is due to the different stoichiometric requirements and heating values of the two fuels. The increase in demand for $H_2$ and $O_2$ with an increase in the sulphide content of the ore is consistent with previous figures.

Fig. 19a presents the extent to which the load of the ASU is reduced after integration of the HyS cycle with the copper production plant via Scenario 1 as a function of the capacity factor of the HyS cycle. Note that the capacity factor is always less than 100% due to the need to accommodate both seasonal and weather-based variability of the solar resource (Kueh et al., 2015). It can be seen that this fraction varies from ~52% to ~71% for capacity factors of 65% to 85%, respectively. Due to operational and economic limitations it is not possible to fully avoid the need for an ASU since it brings the requirement for additional CAPEX in a new plant and OPEX in a new plant or retrofit. Alternatively, the equivalent energy for extra $H_2$ produced ( ~96 mole% purity and LHV=~87 MJ/kg) in Scenario 2 per tonne of copper product is depicted in Fig. 19b. The error bars in Fig. 19a and b represent the effect of variations in the ore sulphide content on the reported parameters.

### 4.3. *The potential in $CO_2$ emissions reduction*

Table 5 presents the assumptions used to calculate the potential for the HyS cycle to mitigate $CO_2$ emissions from copper production based on the situation relevant to Olympic Dam in South Australia. For this plant, electricity is presently drawn from the South Australian (SA) grid, which already has an estimated 60% penetration of renewable energy

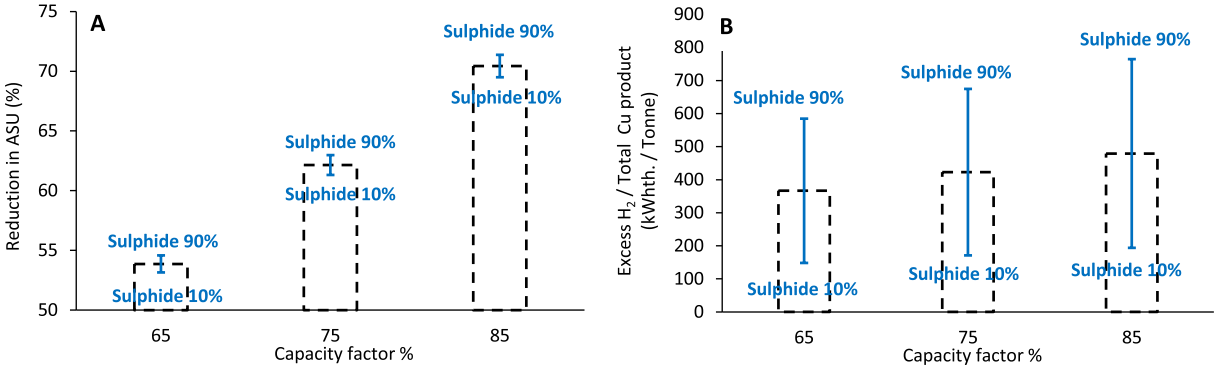


**Fig. 19.** The dependence on the capacity factor of the HyS plant of A) the demand reduction of the air separation unit after integrating the copper production plant with the HyS cycle via Scenario 1 as a function of the capacity factor. B) The fractional excess hydrogen produced after integrating the copper production plant with the HyS cycle via Scenario 2.

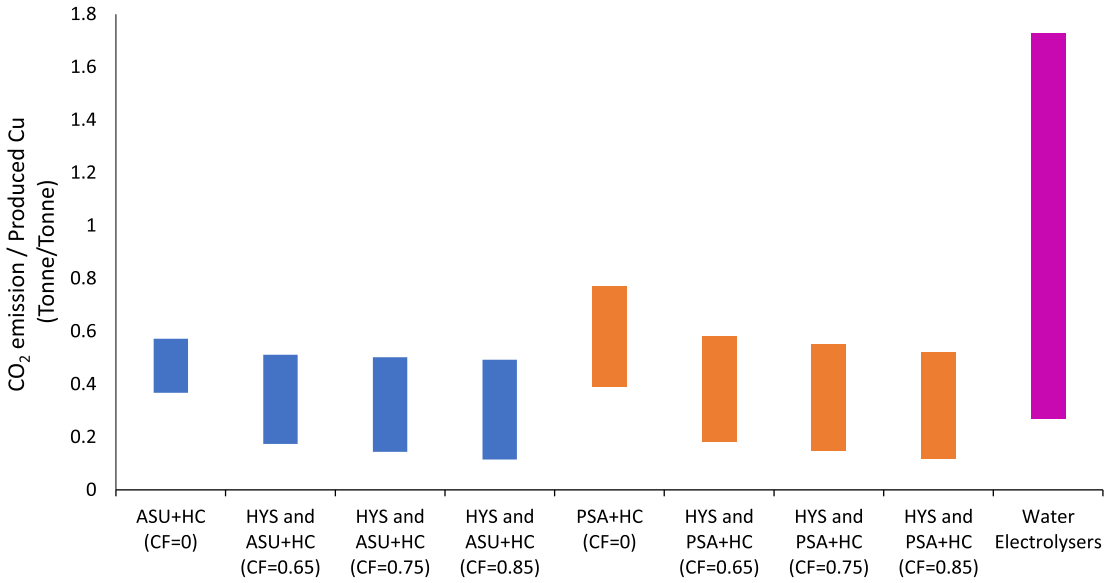


**Fig. 20.** The estimated intensity of $CO_2$ emissions from the pyro furnaces and sulphuric acid plants in the copper production plant for the cases before (capacity factor, CF = 0) and after (CF = 65, 75 and 85) the integration with the HyS cycle. Also shown is the emission from *in-situ* electrolysers supplied from the South Australian grid, as estimated using Table 5. The range of values corresponds to the upper and lower bounds of emissions intensity of the SA grid in 2020, while the copper concentration is set for the conditions that apply in Olympic Dam (where ~80% of Cu is refined through the pyro pathway), Australia.

**Table 6**
Assumptions which were used to evaluate the $CO_2$ emission intensity for data shown in Fig. 20.

| Specification | Unit | Min. | Max. | Ave. | Remarks |
|---|---|---|---|---|---|
| e-CO2 emission of grid electricity | $tCO_2$ / $MWh_{el}$ | 0.09 | 0.58 | 0.34 | AEMO (SA, 2020) [48] |
| ASU electricity consumption (70% mole oxygen purity) | $kWh_{el}$ / $tO_2$ | – | – | 200 | The value is taken from [49,50] |
| PSA electricity consumption (70% mole oxygen purity) | $kWh_{el}$ / $tO_2$ | – | – | 500 | The value is taken from [50] |
| Required $O_2$ in Cu production (ASU or HyS) | $tO_2$ / $tCu_{Pyro}$ | 0.93 | 1.15 | 1.03 | Simulation result (per tonne of refined Cu product via Pyro.) |
| Produced $CO_2$ because of HC burning | $tCO_2$ / $tCu_{Pyro}$ | 7.96 | 9.96 | 8.73 | Simulation result (per tonne of refined Cu product via Pyro.) |
| Electricity consumption (HyS cycle) | $MWh_{el}$ / $tO_2$ | 1.30 | 1.36 | 1.33 | Simulation result |
| Electricity consumption of electrolysers | $MWh_{el}$ / $tO_2$ | – | – | 5 | The value is taken from [51] |

[37]. Hence, this grid's $CO_2$ emissions intensity in 2020 was ~0.09–0.58 tonnes of $CO_2$ per $MWh_{el}$ [48].

Fig. 20 presents the calculated range of $CO_2$ emissions intensity for the current process compared to a series of technology options used to meet the demand for $H_2$ and $O_2$ for the pyro furnaces and the acid units in the copper processing plant for different capacity factors using the assumptions provided in Table 5. Here the ASU + HC and PSA + HC series refer to the use of hydrocarbon fuels (HC), together with the oxygen being produced from ASU from the SA electrical grid or oxygen produced via pressure swing adsorption method (PSA). The water electrolysis bar represents the case in which the electricity from the grid (with the assumptions in Table 5) is used to provide the energy for the oxygen and hydrogen on-site.

**Table 7**
Assumptions were used to estimate the economics of the integration of the copper production process with the HyS cycle via scenarios 1 and 2.

| Specification | Value | Unit | Remarks |
|---|---|---|---|
| The estimated cost of copper production | 4500 | Au $/tCu | Both open pit and underground mining [7] |
| Percentage of the total cost related to Pyro. and acid plant | 12% ± 3% | – | Both open pit and underground mining [7] |
| Cost component of HC fuel, ASU and electricity in Pyro. and acid plant | 20 – 50% | – | This is a fraction of the total operating cost of Pyro. and acid plant based on tables 6-8, Chapter 22 [7] |
| The estimated cost of wholesale LPG | 0.68 ± 20% | Au$/L | The value is used to estimate Cu production cost at Olympic Dam [52] |
| The estimated cost of wholesale fuel oil | 1.1 ± 20% | Au$/L | The value is used to estimate Cu production cost at Olympic Dam [52] |
| The estimated cost of wholesale electricity | 65 ± 5% | Au $/MWh | The value is used to estimate Cu production cost at Olympic Dam [48] |
| The estimated cost of $O_2$ from ASU | 70 ± 5% | Au $/$tO_2$ | The value is used to estimate Cu production cost at Olympic Dam [49] |
| The estimated cost of $H_2$ production via the HyS cycle | 5.1 ± 24% | Au$/kg | [29] |
| The HyS cycle production capacity | 100 | $tH_2$/day | [29] |
| The capacity factor of the HyS cycle | 0.75 | – | [29] |
| Energy storage capacity | 13 | h | [14,29] |
| Cost estimation exponents | 0.6 ± 0.1 | – | The exponents [53] are used to adjust the evaluated cost of hydrogen for 100 tonnes per day to the estimated hydrogen demands via scenarios 1 and 2. Note that the required hydrogen is taken from the simulation results (Fig. 16) |
| Revenue from extra hydrogen produced via Scenario 2 | 4 | AUD $/kg | Competitive with the CSIRO 2025 cost for green H2 via PEM and AE [54] |

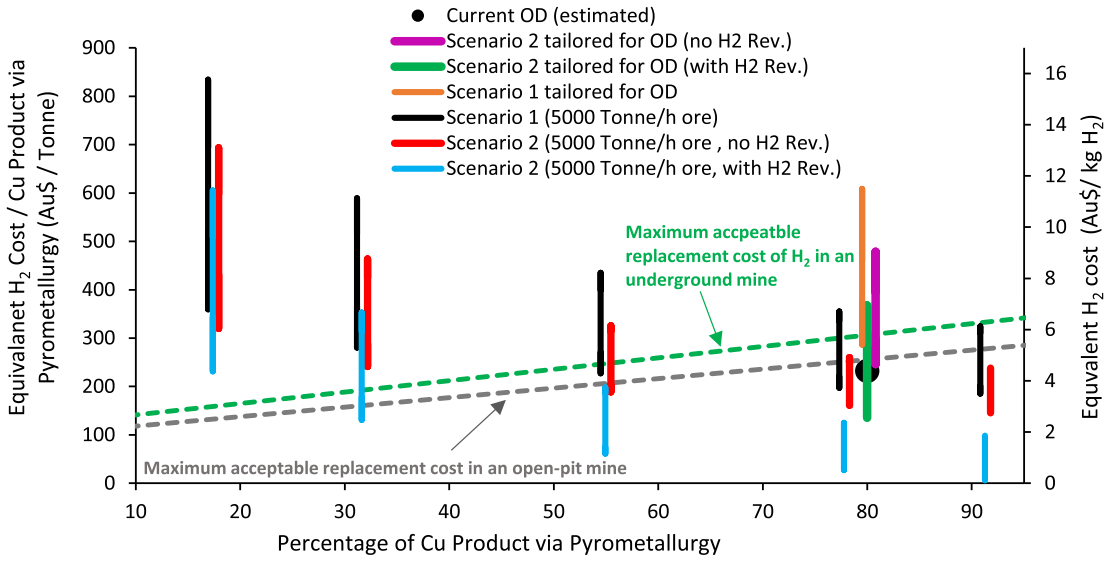


**Fig. 21.** Estimated cost of hydrogen production in the HyS cycle and its unitlisation in furnaces of a copper plant through Scenario 1, Scenario 2 without $H_2$ revenue and Scenario 2 with $H_2$ revenue (4 Au$/kg $H_2$) for different fraction of copper product via pyrometallurgy.

The results in Fig. 20 show that the integration of the copper production plant with the HyS cycle offers the highest potential to decrease the $CO_2$ emissions by more than 50% (blue bars). The $CO_2$ emissions of the grid significantly impacts the potential decrease in the emission after integrating the copper production plant with the HyS cycle. For example, with the minimum value of grid $CO_2$ emissions (0.09 $tCO_2$ / $MWh_{el}$), the reduction in $CO_2$ emissions from integrating the copper plant with the HyS cycle is comparable with that from electrolysis. It should also be noted that both the electrolysis units and the HyS cycle can further reduce emissions intensity. For the HyS cycle, this would require thermal storage, or chemical storage (sulphuric acid, oxygen and hydrogen storage) or a combination of both, whilst for the electrolysis, this would require increased penetration of renewable energy into the grid. However, the investigation of these options is beyond the scope of the present research.

### 4.4. Preliminary assessment on the economics of integration

The economic assessment was based on a previous economic assessment of the HyS cycle [29], which estimated a hydrogen production cost of ~5.1 ± 1.2 Au$/kg $H_2$ (for a capacity of 100 tonnes per day). Table 6 lists this, together with the other assumptions that were used in the economic assessment.

Fig. 21 presents the estimated equivalent cost of hydrogen per tonne of the pyrometallurgical copper product after integration of the HyS cycle with a copper plant (i.e. from replacing both the HC fuel and the ASU demands of the copper plant with $O_2$ and $H_2$ from the solar thermal and HyS cycle). Data are presented for three cases namely; Scenario 1, Scenario 2 without $H_2$ revenue and Scenario 2 with $H_2$ revenue (4 Au $/kg $H_2$). This price is competitive with (i.e. slightly below) the estimated production costs of green hydrogen via both PEM and alkaline electrolysis in Australia by 2025 [54]. This price is also estimated to be economical for heavy trucks, which is a likely application in the mining sector. Also shown is the cost estimation using the model of the current operating cost of pyrometallurgical production of copper at Olympic Dam (OD) (the black circle). Note that also the three aforementioned scenarios tailored for OD estimated capacity (1900 tonne/h) are shown in Fig. 21.

Fig. 21 also presents two sloped dashed lines, which correspond to the estimated maximum viable cost of hydrogen to justify replacing the current fuel and air on economic grounds alone in a conventional copper production plant supplied either for an underground or an open-pit mine. It can be seen that, for sulphide fractions of the copper-containing ore of 10%, 25%, 50%, and 90% (which corresponds to 17%, 31%, 55%, 77%, and 91% of Cu product via pyrometallurgy), the maximum cost of hydrogen per tonne of pyrometallurgical copper product in Au$ should be less than 157, 191, 246, 300 and 332 for underground mines and 132, 160, 205, 250 and 277 for open-pit mines without any premium for low-carbon products, respectively. The maximum value of each series in Fig. 21 corresponds to n = 0.5 (scale exponent) and 6.3 Au$/ kg $H_2$ for HyS cycle capacity of 100 tonnes per day (row 8 in Table 6), while the corresponding minimum is for n = 0.7 and 3.9 Au$/ kg $H_2$. The second vertical axis in Fig. 21 reports the equivalent values in Au$/ kg $H_2$.

It is evident from Fig. 21 that an increase in the fraction of the copper produced via pyrometallurgy leads to a reduction in the copper production cost after integration with the HyS cycle. Furthermore, it is estimated to be economically favourable to employ the HyS cycle via Scenario 2, where more than 70% of the copper is processed via the pyrometallurgical pathway for underground and open-pit mining without any carbon price or low-carbon premium.

It should be noted that some data in Fig. 21 are related to plants with a capacity of 5000 tonne ore/h, and therefore since the capacity of OD is about 2.6 times less than the original flowsheet, all the employed scenarios predicted a high cost for the hydrogen replacements. Nevertheless, Scenario 2, with revenue from the excess $H_2$, could provide a distinctly lower price than the cost estimated for the conventional copper production using HC and ASU at Olympic Dam (the black circle in Fig. 21).

## 5. Conclusions

With this model it is estimated that the integration of the renewable HyS cycle into copper production is economically favourable even without any carbon price or low-carbon premium for those cases where more than 70% of the copper is processed via the pyrometallurgical pathway (i.e., for ores of more than ~50% sulphide) for both underground and open-pit mining. This estimate is based on the assumption that the excess hydrogen is valued at AUD$4/kg, e.g., for transportation in the mine, which is typical of the estimated cost for green hydrogen in 2025 [54]. The use of a premium and/or the further development of the HyS cycle to continue to lower its production cost would further increase the viability and/or allow its use for ores with a lower sulphide content.

The viability is also found to be greatest for Scenario 2, in which the

HyS cycle is sized to meet the oxygen demand of the copper plant rather than the hydrogen demand needed to replace the hydrocarbon fuel. The level of $CO_2$ mitigation from this approach is also greater than would occur using electrolysis if fed from a non-renewable electrical grid, such as that with current emissions intensity. While zero net emissions are potentially possible with either HyS or electrolysis, both require further developments in technology over what is currently available. Hence further research is justified both to continue the upscaling and further development of the HyS cycle, and to explore further options for supplying a copper production site with oygen and hydrogen from various renewable water-splitting routes, including electrolysis.

## CRediT authorship contribution statement

**Ahmad Seyfaee:** Conceptualization, Investigation, Methodology, Software, Data curation, Formal analysis, Validation, Visualization, Writing – original draft, Writing - review & editing, Resources, Project administration. **Mehdi Jafarian:** Conceptualization, Investigation, Methodology, Software, Data curation, Formal analysis, Validation, Visualization, Writing – original draft, Writing - review & editing, Resources, Project administration, Supervision. **Gkiokchan Moumin:** Conceptualization, Investigation, Data curation, Validation, Writing - review & editing. **Dennis Thomey:** Data curation, Visualization, Writing - review & editing. **Claudio Corgnale:** Writing - review & editing, Investigation, Visualization, Writing - review & editing. **Christian Sattler:** Investigation, Writing - review & editing, Supervision. **Graham J. Nathan:** Conceptualization, Supervision, Formal analysis, Methodology, Writing – original draft, Writing - review & editing, Supervision, Funding acquisition.

## Declaration of Competing Interest

The authors declare that they have no known competing financial interests or personal relationships that could have appeared to influence the work reported in this paper.

## Acknowledgement

This research was performed as part of the Australian Solar Thermal Research Initiative (ASTRI), a project supported by the Australian Government, through the Australian Renewable Energy Agency (ARENA), ARENA 1-SRI002. The views expressed herein are not necessarily the views of the Australian Government, and the Australian Government does not accept responsibility for any information or advice contained herein. The author would also like to acknowledge the financial support of ARENA IEP MI5 program, enabling the paper to be open access. The valuable feedback on the original draft by the anonymous reviewers is also gratefully acknowledged.

## Appendix A. Supplementary data

Supplementary data to this article can be found online at https://doi.org/10.1016/j.enconman.2021.114832.

## References

[1] Rötzer N, Schmidt M. Historical, current, and future energy demand from global copper production and its impact on climate change. Resources 2020;9(4):44. https://doi.org/10.3390/resources9040044.
[2] Moreno-Leiva S, Haas J, Junne T, Valencia F, Godin H, Kracht W, et al. Renewable energy in copper production: A review on systems design and methodological approaches. J Clean Prod [Internet]. 2020 Feb;246:118978. Available from: doi: 10.1016/j.jclepro.2019.118978.
[3] Ekman Nilsson A, Macias Aragonés M, Arroyo Torralvo F, Dunon V, Angel H, Komnitsas K, et al. A review of the carbon footprint of Cu and Zn production from primary and secondary sources. Minerals 2017;7(9):168. https://doi.org/10.3390/min7090168.
[4] Mudd GM, Memary R, Northey SA, Giurco D, Mohr S, Mason L. CLUSTER RESEARCH REPORT No. 1.12 Future Greenhouse Gas Emissions from Copper Mining: Assessing Clean Energy Scenarios. 2012;(1):1–32. Available from: www.isf.uts.edu.au.
[5] Sohn HY, Malfliet A, Scheunis L, Jones PT, Blanpain B. Copper Production. Vol. 3, Treatise on Process Metallurgy. 2014. 534–624 p.
[6] Bacon G, Mihaylov I. Solvent extraction as an enabling technology in the nickel industry Coming of age in copper solvent extraction. J South African Inst Min Metall. 2002;(December):435–44.
[7] E. SM, J. KM, G. DW. Extractive metallurgy of Copper [Internet]. Elsevier. 2011. Available from: http://www.elsevier.com/locate/scp.
[8] Tow T, Yusup Y, Wei L. Heavy Metal Ion Extraction Using Organic Solvents: An Application of the Equilibrium Slope Method. Stoichiom Res - Importance Quant Biomed. 2012;(March).
[9] Gallardo FI, Monforti Ferrario A, Lamagna M, Bocci E, Astiaso Garcia D, Baeza-Jeria TE. A Techno-Economic Analysis of solar hydrogen production by electrolysis in the north of Chile and the case of exportation from Atacama Desert to Japan. Int J Hydrogen Energy [Internet]. 2020;(xxxx). Available from: https://doi.org/10.1016/j.ijhydene.2020.07.050.
[10] Röben FTC, Schöne N, Bau U, Reuter MA, Dahmen M, Bardow A. Decarbonizing copper production by power-to-hydrogen: A techno-economic analysis. J Clean Prod. 2021;306.
[11] Brown NR, Revankar ST. A review of catalytic sulfur (VI) oxide decomposition experiments. Int J Hydrogen Energy [Internet]. 2012;37(3):2685–98. Available from: doi: 10.1016/j.ijhydene.2011.10.054.
[12] Hinkley J, Agrafiotis C. Solar thermal energy and its conversion to solar fuels via thermochemical processes [Internet]. Polygeneration with Polystorage: For Chemical and Energy Hubs. Elsevier Inc.; 2018. 247–286 p. Available from: doi: 10.1016/B978-0-12-813306-4.00009-4.
[13] Thomey D, De Oliveira L, Säck JP, Roeb M, Sattler C. Development and test of a solar reactor for decomposition of sulphuric acid in thermochemical hydrogen production. Int J Hydrogen Energy 2012;37(21):16615–22.
[14] Gorensek MB, Corgnale C, Summers WA. Development of the hybrid sulfur cycle for use with concentrated solar heat. I. Conceptual design. Int J Hydrogen Energy 2017;42(33):20939–54.
[15] Jung YH, Jeong YH. Development of the once-through hybrid sulfur process for nuclear hydrogen production. Int J Hydrogen Energy [Internet]. 2010;35(22):12255–67. Available from: doi: 10.1016/j.ijhydene.2010.07.168.
[16] Niehoff AG, Botero NB, Acharya A, Thomey D, Roeb M, Sattler C, et al. Process modelling and heat management of the solar hybrid sulfur cycle. Int J Hydrogen Energy [Internet]. 2015;40(13):4461–73. Available from: doi: 10.1016/j.ijhydene.2015.01.168.
[17] Bayer Botero N, Thomey D, Guerra Niehoff A, Roeb M, Sattler C, Pitz-Paal R. Modelling and scaling analysis of a solar reactor for sulphuric acid cracking in a hybrid sulphur cycle process for thermochemical hydrogen production. Int J Hydrogen Energy [Internet]. 2016;41(19):8008–19. Available from: doi: 10.1016/j.ijhydene.2015.11.088.
[18] Nathan GJ, Jafarian M, Dally BB, Saw WL, Ashman PJ, Hu E, et al. Solar thermal hybrids for combustion power plant: a growing opportunity. Prog Energy Combust Sci 2018;64:4–28.
[19] Bayon A, Bader R, Jafarian M, Fedunik-Hofman L, Sun Y, Hinkley J, et al. Techno-economic assessment of solid–gas thermochemical energy storage systems for solar thermal power applications. Energy [Internet]. 2018;149:473–84. Available from: doi: 10.1016/j.energy.2017.11.084.
[20] Corgnale C, Gorensek MB, Summers WA. Review of sulfuric acid decomposition processes for sulfur-based thermochemical hydrogen production cycles. Processes. 2020;8(11):1–22.
[21] Kojo I V., Storch H. Copper production with outokumpu flash smelting: An update. 2006 TMS Fall Extr Process Div Sohn Int Symp. 2006;8(June):225–38.
[22] Wilkomirsky I, Parra R, Parada F, Balladares E. Continuous converting of copper matte to blister copper in a high-intensity molten-layer reactor. JOM 2014;66(9):1687–93.
[23] Lassouane F, Menia S, Khellaf A. An overview of the hybrid sulfur cycle process for solar hydrogen production. 3rd Int Symp Environ Friendly Energies Appl EFEA 2014. 2014.
[24] Jafarian M, Arjomandi M, Nathan GJ. Thermodynamic potential of molten copper oxide for high temperature solar energy storage and oxygen production. Appl Energy [Internet]. 2017;201:69–83. Available from: doi: 10.1016/j.apenergy.2017.05.049.
[25] Jafarian M, Arjomandi M, Nathan GJ. The energetic performance of a novel hybrid solar thermal & chemical looping combustion plant. Appl Energy [Internet]. 2014;132:74–85. Available from: doi: 10.1016/j.apenergy.2014.06.052.
[26] Jafarian M, Arjomandi M, Nathan GJ. Influence of the type of oxygen carriers on the performance of a hybrid solar chemical looping combustion system. Energy Fuels 2014;28(5):2914–24.
[27] Jafarian M, Arjomandi M, Nathan GJ. A hybrid solar chemical looping combustion system with a high solar share. Appl Energy [Internet]. 2014;126:69–77. Available from: doi: 10.1016/j.apenergy.2014.03.071.
[28] Corgnale C, Shimpalee S, Gorensek MB, Satjaritanun P, Weidner JW, Summers WA. Numerical modeling of a bayonet heat exchanger-based reactor for sulfuric acid decomposition in thermochemical hydrogen production processes. Int J Hydrogen Energy [Internet]. 2017;42(32):20463–72. Available from: doi: 10.1016/j.ijhydene.2017.06.216.
[29] Corgnale C, Summers WA. Solar hydrogen production by the Hybrid Sulfur process. Int J Hydrogen Energy [Internet]. 2011;36(18):11604–19. Available from: doi: 10.1016/j.ijhydene.2011.05.173.

[30] Barin I, Platzki G. Thermochemical data of pure substances [Internet]. Third Edit. Vol. 55. New York; 1997. Available from: https://linkinghub.elsevier.com/retrieve/pii/S0165242796056322.
[31] Ballantyne GR, Powell MS, Tiang M. Proportion of energy attributable to comminution. Proc 11th Australas Inst Min Metall Mill Oper Conf. 2012;(October):25–30.
[32] Mudd GM. Prediction of Greenhouse Gas Emissions for the Olympic Dam Mega-Expansion. 2009;(April):1–13.
[33] Alexander DJ, Wigley P. Flotation circuit analysis at WMC Ltd Olympic Dam Operation. 8th Mill Oper Conf [Internet]. 2003;(July):41–51. Available from: https://apps.webofknowledge.com/full_record.do?product=UA&search_mode=GeneralSearch&qid=31&SID=F2T4mXddXK9AcD9TAX2&page=12&doc=593&cacheurlFromRightClick=no.
[34] Vignes A. Extractive metallurgy 2: metallurgical reaction processes. John Wiley & Sons; 2013.
[35] Coursol P, Mackey PJ. Energy consumption in copper sulphide smelting. Mater Sci 2010:649–68.
[36] Rich DW. Smelting practice at Olympic Dam. Conf Ser – Australas Inst Min Metall. 1993;(April):207–15.
[37] Cargill R, Freeman N, Gilbertson R. Metal balance for olympic dam using a standard industrial software package. Australas Inst Min Metall Publ Ser 2002;8:149–56.
[38] King MJ, Daveport WG, Moats MS. Sulphuric Acid Manufacture Analysis, Control & Optimization. 2013.
[39] Nilay Kumar Sarker TAK. Simulation of the Production of Sulfuric Acid from a Sulfur-burning Single-absorption Contact Sulfuric Acid Plant. Int J Emerg Technol Innov Res JETIR. 2015;Vol. 2-I(Vol. 2-Issue 6 (July-2015)):2006–11.
[40] Cheng CY, Urbani M. The recovery of nickel and cobalt from leach solutions by solvent extraction. 2005;(January 2005).
[41] Macmillan E, Ehrig K, Liebezeit V, Kittler P, Lower C. Use of geometallurgy to predict tailings leach acid consumption at Olympic Dam. GeoMet 2011 - 1st AusIMM Int Geometallurgy Conf 2011. 2011;(September):93–102.
[42] Girgin I, Resources N. Comparative H 2 SO 4 and H 2 SO 4 + H 2 O 2 leaching of a Turkish lateritic nickel ore. Impc 2014;2014:1–10.
[43] Gri J, Ehrig K. Using existing data to improve the delineation of ore at the Olympic Dam Fe-oxide Cu-U-Au-Ag deposit. 2017;(September).
[44] BHP. Existing operation (Olympic Dam Copper refinery). 2009.
[45] Boisvert JB, Rossi ME, Ehrig K, Deutsch CV. Geometallurgical modeling at olympic dam mine, South Australia. Math Geosci. 2013;45(8):901–25.
[46] Ballantyne GR, Powell MS. Benchmarking comminution energy consumption for the processing of copper and gold ores. Miner Eng 2014;65:109–14.
[47] Crundwell F, Moats M, Robinson T, Ramachandran V, Davenport W. Extractive Metallurgy of Nickel and Cobalt. Extractive Metallurgy of Nickel,Cobalt and Platinim Group Metals. 2011. 489–534 p.
[48] AEMO. AEMO | Carbon Dioxide Equivalent Intensity Index [Internet]. [cited 2021 Mar 9]. Available from: https://aemo.com.au/en/energy-systems/electricity/national-electricity-market-nem/market-operations/settlements-and-payments/settlements/carbon-dioxide-equivalent-intensity-index.
[49] Belaissaouia Bouchra, Moullec Yann Le, Hagi Hayato, Favre Eric. Energy Efficiency of Oxygen Enriched Air Production Technologies: Cryogeny vs Membranes. Energy Procedia [Internet]. 2014;63:497–503. Available from: www.sciencedirect.com.
[50] Banaszkiewicz T, Chorowski M, Gizicki W. Comparative analysis of cryogenic and PTSA technologies for systems of oxygen production. AIP Conf Proc. 2014;1573(February 2015):1373–8.
[51] Moore J. Thermal Hydrogen: An emissions free hydrocarbon economy. Int J Hydrogen Energy [Internet]. 2017;42(17):12047–63. Available from: https://doi.org/10.1016/j.ijhydene.2017.03.182.
[52] Home | Australian Institute of Petroleum [Internet]. [cited 2021 Mar 20]. Available from: https://www.aip.com.au/.
[53] Gavin T, Ray S. Chemical Engineering Design Principles, Practice and Economics of Plant and Process Design. 2nd ed. 2012.
[54] Bruce S, Temminghoff M, Hayward J, Schmidt E, Munnings C, Palfreyman D, et al. National Hydrogen Roadmap. 2019;116. Available from: www.csiro.au.